ELECTROMAGNETIC WAVE SCATTERING AND SOME INSTRUMENTATION OF ITS ACOUSTIC SIMULATION FACILITY

by

TAKUYA KOIZUMI

B. E., Fukui University, 1958

A MASTER'S THESIS

submitted in partial fulfillment of the

requirements for the degree

MASTER OF SCIENCE

Department of Electrical Engineering

KANSAS STATE UNIVERSITY
Manhattan, Kansas

1964

Approved by:

Harhajan S. Hayre
Major Professor

TABLE OF CONTENTS

INTRODUCTION

A great amount of research effort has been expended on the problem of electromagnetic back-scatter. Theoretical, experimental, and laboratory simulation work on this subject is now in progress at various international facilities. Acoustic simulation, although not suitable for simulation of some polarizations, is considered to be a very inexpensive and useful method in this field. The simulated return is generally of the form of a randomly varying amplitude pulse, which is then sampled and analyzed statistically. Therefore an electronic sampler offers a great saving of time in such an analysis. It was therefore necessary to design and build such a device.

The problem of scattering of electromagnetic wave from almost plane inhomogeneous terrain with randomly varying impedance-like function is discussed in the first part. An electronic sampling circuit for the acoustic simulation facility of the Department of Electrical Engineering, Kansas State University, is discussed in the second part.

SCATTERING OF ELECTROMAGNETIC WAVE FROM ALMOST PLANE INHOMOGENEOUS TERRAIN WITH RANDOMLY VARYING IMPEDANCE

A number of papers on the subject of calculation of electromagnetic back-scatter from a rough surface have been published in the last decade (Davies, 1954; Moore, 1957; Cooper, 1958; Hayre, 1961). Usually a statistical model of rough surface is employed. For instance, the surface heights of natural terrain have been shown to be often normally distributed about the mean ground level. The scattering of an electromagnetic wave, incident on such a rough surface, can be calculated in terms of its statistical parameters, the wavelength and the angle of incidence.

There are basically two methods of attack: one relies on the statistical description of a rough surface, and employs either the Kirchhoff-Huygens approximation or Maxwell's equations; whereas the other method incorporates the random roughness of a surface in its impedance while assuming its surface to be a plane surface (Felson, 1962; Fock, 1956; Isakovich, 1956; and Senior, 1960). A modification of the latter is studied exclusively in this work.

Derivation of Rayleigh Conditional Probability Density Function

The conditional probability density of a Rayleigh distributed variable R is used to obtain an expression for the average received power from the target terrain and its derivation is given in the following paragraph.

Let R denote a complex quantity and let its real and imaginary components be u and v respectively. Then,

$$R = u + jv = |R| \cos\theta + j |R| \sin\theta$$

$$|R|^2 = u^2 + v^2 \qquad (1)$$

It is assumed that u and v are normally distributed with $(0,\sigma)$, and their probability density functions are

$$p(u) = \frac{1}{\sqrt{2\pi\sigma^2}} \exp\left(-\frac{u^2}{2\sigma^2}\right), -\infty < u < +\infty \tag{2}$$

$$p(v) = \frac{1}{\sqrt{2\pi\sigma^2}} \exp\left(-\frac{v^2}{2\sigma^2}\right), -\infty < v < +\infty \tag{3}$$

If u and v are independent random variables, then their joint probability density is

$$p(u,v) = p(u) \cdot p(v) = \frac{1}{2\pi\sigma^2} \exp\left(-\frac{u^2 + v^2}{2\sigma^2}\right) \tag{4}$$

If a transformation from rectangular coordinates (u,v) to polar coordinates (R,θ) is made, $q(R,\theta)$, the probability density function for the polar coordinates, is given as

$$q(R,\theta)dR\ d\theta = p(u,v)du\ dv \tag{5}$$

Transforming differential areas yields

$$du\ dv = R\ dR\ d\theta \tag{6}$$

Combination of Eqs. (4), (5), and (6) gives

$$q(R,\theta)dR\ d\theta = \frac{Re^{-R^2/2\sigma^2}}{2\pi\sigma^2}\ dR\ d\theta\ ,\ R \geq 0 \tag{7}$$

and

$$q(R,\theta) = \frac{R}{2\pi\sigma^2} \exp\left(-R^2/2\sigma^2\right), 0 < \theta < 2\pi \tag{8}$$

The marginal density function q(R) is then calculated by integrating Eq. (8) over θ, for $0 < \theta < 2\pi$ (Bendat, 1958), as

$$q(R) = \int_0^{2\pi} q(R,\theta)d\theta = \frac{R}{\sigma^2} \exp\left(-\frac{R^2}{2\sigma^2}\right) \tag{9}$$

Let (u_1, v_1) and (u_2, v_2) denote the orthogonal components of R at the points (x_1, y_1) and (x_2, y_2) respectively. The components are normally distributed with mean zero and standard deviation σ, and are independent of each other. It follows from the central limit theorem that the four random variables u_1, v_1, u_2, v_2 have a four-dimensional normal density function as

$$f(u_1, v_1, u_2, v_2) = (2\pi)^{-2} |M|^{1/2} \exp\left(-\frac{1}{2|M|} \sum_{i,j=1}^{2} M_{ij} u_i v_j\right) \quad (10)$$

Their second moments are

$$\overline{u_1^2} = \overline{v_1^2} = \overline{u_2^2} = \overline{v_2^2} = \sigma^2 \quad (11)$$

$$\overline{u_1 v_1} = \overline{u_2 v_2} = 0 \quad (12)$$

$$\overline{u_1 u_2} = \overline{v_1 v_2} = \mu \text{ (autocorrelation of u and v)} \quad (13)$$

$$\overline{u_1 v_2} = \overline{u_2 v_1} = 0. \quad (14)$$

The moment matrix M for these variables is

$$M = \begin{bmatrix} \sigma^2 & 0 & \mu & 0 \\ 0 & \sigma^2 & 0 & \mu \\ \mu & 0 & \sigma^2 & 0 \\ 0 & \mu & 0 & \sigma^2 \end{bmatrix} \quad (15)$$

The cofactors of the determinant $|M|$ are

$$M_{11} = M_{22} = M_{33} = M_{44} = \sigma^2(\sigma^4 - \mu^2) = \sigma^2 A, \text{ where } A = (\sigma^4 - \mu^2). \quad (16)$$

$$M_{13} = M_{24} = -\mu A \quad (17)$$

$$M_{14} = M_{23} = 0 = M_{12} = M_{34} \quad (18)$$

$$|M| = A^2 \quad (19)$$

The joint probability density of the four random variables is therefore

$$f(u_1,v_1,u_2,v_2) = \frac{1}{4\pi^2 A} \exp\left[-\frac{1}{2A}\left\{\sigma^2(u_1^2 + v_1^2 + u_2^2 + v_2^2) - 2\mu(u_1u_2 + v_1v_2)\right\}\right]. \tag{20}$$

The joint probability density of R_1 and R_2 (Rice, 1944) is

$$f(R_1, R_2) = \frac{R_1R_2}{A} I_0\left(\frac{R_1R_2}{A}\mu\right) \exp\left[-\frac{\sigma^2}{2A}(R_1^2 + R_2^2)\right] \tag{21}$$

where I_0 is the Bessel function of the first kind with imaginary argument.

The conditional probability density of R_2 given R_1 can now be calculated from Eq. (9) and (20) as

$$f(R_2/R_1, \vec{r}) = \frac{f(R_1, R_2)}{q(R_1)} = \frac{f(R_1, R_2)}{\frac{R_1}{\sigma^2}\exp\left(-\frac{R_1^2}{2\sigma^2}\right)}$$

$$= \frac{\sigma^2 R_2}{A} I_0\left(\frac{R_1R_2}{A}\mu\right) \exp\left[R_1^2\left(\frac{1}{2\sigma^2} - \frac{\sigma^2}{2A}\right) - \frac{\sigma^2}{2A} R_2^2\right], \tag{22}$$

where r is a distance between the points (x_1, y_1) and (x_2, y_2).

Average Received Power Scattered from the Terrain

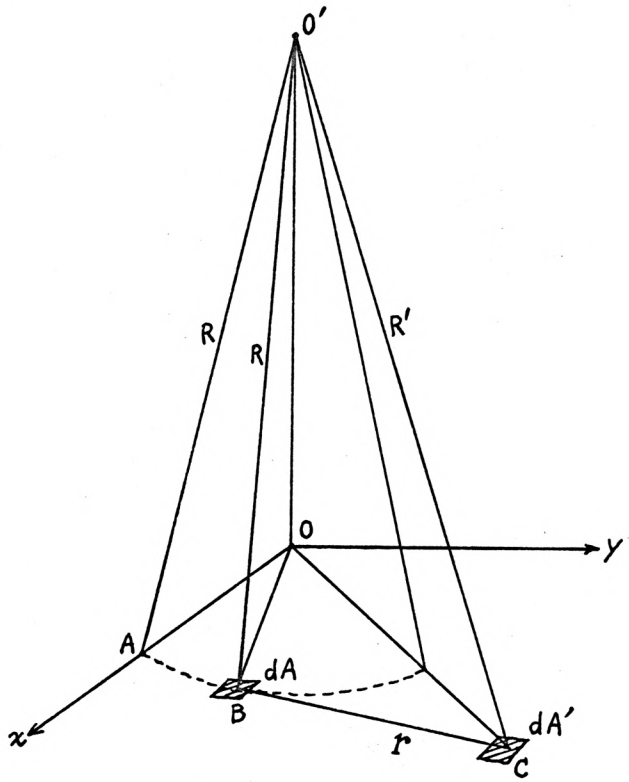

$\overline{BC} = r$

$\overline{O'A} = \overline{O'B} = R$

$\overline{O'C} = R'$

$\angle AOB = \phi$, $\angle AOC = \phi'$

$\angle BO'O = \theta$, $\angle CO'O = \theta'$

$\angle AO'B = \psi$, $\angle AO'C = \psi'$

Figure 1A. Geometry of the Problem.

The electric field E at the receiver O' due to reflection from a finite conductivity ground in Figure 1A can be obtained by using the Kirchhoff-Huygens principle

$$E = \iint \frac{1}{\lambda R}(I_s \eta)^{1/2} V \cos\theta \quad \exp(-j2kR)\, dA \quad \text{(Hayre, 1961)} \qquad (23)$$

where $I_s = P_T G/(4\pi R^2)$

η = intrinsic impedance of free space

dA = area element on the terrain ($= RdRd\psi/\sin\theta$)

P_T = power transmitted

R = range

G = antenna gain

λ = wavelength

V = reflection coefficient of area element dA

$k = 2\pi/\lambda$.

The following assumptions have been made in applying Huygens' principle to the problem of the geometry shown in Figure 1A.

i) The terrain has a randomly varying resistive impedance, which yields the same attenuation as would the various points of a rough surface at randomly varying elevations.

ii) The radiation from a particular small area on the terrain is isotropic.

iii) The antenna gain is essentially uniform for $-\theta_0 < \theta < +\theta_0$, and zero outside of this range.

The expression for E in Eq. (23) is modified for pulse radar using a pulse width of τ seconds to yield

$$E = \frac{1}{\lambda} \int_{-\frac{c\tau}{4}}^{+\frac{c\tau}{4}} \int_{-\theta_0}^{\theta_0} \frac{\cot\theta}{R} \left(\frac{P_T G \gamma}{4\pi R^2}\right)^{1/2} V \exp(-j2kR)\, dR\, d\psi \qquad (24)$$

where c = velocity of propagation

τ = pulse width

$2\theta_0$ = beam width of the antenna

The reflection coefficient V may be expressed as a function of the terrain admittance γ as

$$V = \frac{\cos\theta - \gamma}{\cos\theta + \gamma} \qquad (25)$$

If γ is replaced by the impedance of the terrain $Z = \frac{1}{\gamma}$, Eq. (25) becomes

$$V = \frac{Z \cos\theta - 1}{Z \cos\theta + 1} \tag{26}$$

The received power P_r can be calculated using Poynting's vector definition as

$$P_r = \frac{1}{2} R_e \left[\frac{E E^*}{\eta} \frac{G \lambda^2}{4\pi} \right] \tag{27}$$

where E^* is complex conjugate of E, and R_e represents "Real part of". From Eqs. (23) and (26) one obtains

$$E^* = \int\int \frac{1}{\lambda R'} (I_s' \eta)^{1/2} \cos\theta' \left(\frac{Z' \cos\theta' - 1}{Z' \cos\theta' + 1}\right) \exp(+j2kR')\, dA' \tag{28}$$

On substitution of Eqs. (24) and (28) into Eq. (27), the received power becomes

$$P_r = \frac{P_T G^2}{32\pi^2} R_e \int\int\int\int \frac{\cot\theta \cot\theta'}{R R'} \left(\frac{Z \cos\theta - 1}{Z \cos\theta + 1}\right) \left(\frac{Z' \cos\theta' - 1}{Z' \cos\theta' + 1}\right) \exp\left\{-j2k(R-R')\right\} dR\, dR'\, d\psi\, d\psi' \tag{29}$$

where the primed quantities refer to a point at (R', θ', ψ').

The average received power can now be expressed as

$$\overline{P}_r = \frac{P_T G^2}{32\pi^2} R_e \int\int\int\int \frac{\cot\theta \cot\theta'}{R R'} \overline{\left(\frac{Z \cos\theta - 1}{Z \cos\theta + 1}\right) \left(\frac{Z' \cos\theta' - 1}{Z' \cos\theta' + 1}\right)} \exp\left\{-j2k(R-R')\right\} dR\, dR'\, d\psi\, d\psi' \tag{30}$$

Let $$\left(\frac{Z\cos\theta - 1}{Z\cos\theta + 1}\right)\left(\frac{Z'\cos\theta' - 1}{Z'\cos\theta' + 1}\right) = W. \tag{31}$$

The expression (30) yields the average received power provided that W is averaged over Z and Z' using their probability density functions, assuming $\theta \cong \theta'$ for near vertical incidence. Now W can be expressed as,

$$W = 1 - \frac{2}{t_1 + 1} - \frac{2}{t_2 + 1} + \left(\frac{2}{t_1 + 1}\right)\left(\frac{2}{t_2 + 1}\right) \tag{32}$$

where $t_1 = Z\cos\theta$, and $t_2 = Z'\cos\theta$. (33)

The resistance Z is assumed to have Rayleigh probability density,

$$q(Z) = \frac{Z}{\sigma^2}\exp\left(-\frac{Z^2}{2\sigma^2}\right), \qquad Z \geqq 0. \tag{34}$$

The conditional probability density of Z' at (x_2, y_2) given Z at (x_1, y_1) where $(x_2 - x_1, y_2 - y_1) = \vec{r}$ is obtained from Eq. (22) as

$$f(Z'/Z, \vec{r}) = \frac{\sigma^2 Z'}{A} I_0\left(\frac{Z\,Z'}{A}\mu\right)\exp\left[Z^2\left(\frac{1}{2\sigma^2} - \frac{\sigma^2}{2A}\right) - \frac{\sigma^2}{2A}Z'^2\right] \tag{35}$$

where $A = \sigma^4 - \mu^2$, μ is autocorrelation function which is a function of distance r.

First, W is averaged over Z' using the Eq. (35), as

$$\left[W\right]_{Z'} = \int_0^\infty W\, f(Z' / Z, \vec{r})\,dZ'$$

$$= 1 - \frac{2}{t_1 + 1} + 2\left(\frac{2}{t_1 + 1} - 1\right)\int_0^\infty \frac{1}{t_2 + 1} f(Z' / Z, \vec{r})\,dZ' \tag{36}$$

Let $I_1 = \int_0^\infty \frac{1}{t_2 + 1} f(Z' / Z, \vec{r})dZ'$. (37)

Now solving for I_1, one obtains

$$I_1 = \frac{\sigma^2}{A} \exp\left[Z^2\left(\frac{1}{2\sigma^2} - \frac{\sigma^2}{2A}\right)\right] \int_0^\infty \frac{Z'}{t_2 + 1} I_0\left(\frac{ZZ'}{A}\mu\right) \exp\left(-\frac{\sigma^2}{2A} Z'^2\right)dZ'$$

$$= \frac{\sigma}{\sqrt{A}\cos\theta} \exp\left[Z^2\left(\frac{1}{2\sigma^2} - \frac{\sigma^2}{2A}\right)\right] \int_0^\infty \frac{u}{u + \frac{\sigma}{\sqrt{A}\cos\theta}}$$

$$I_0\left(\frac{Z}{\sigma\sqrt{A}} u\mu\right) \exp\left(-\frac{u^2}{2}\right) du, \quad (38)$$

where $u = \frac{\sigma}{\sqrt{A}} Z'$. (39)

Since $I_0\left(\frac{Z}{\sigma\sqrt{A}} u\mu\right) \cong \frac{\exp\left(\frac{Z}{\sigma\sqrt{A}} u\mu\right)}{\sqrt{2\pi \frac{Z}{\sigma\sqrt{A}} u\mu}}$ (40)

for $\frac{Z}{\sigma\sqrt{A}} u\mu \gg 1$ and $\frac{u}{u + \frac{\sigma}{\sqrt{A}\cos\theta}} < 1$ for all u,

$\exp\left(-\frac{u^2}{2}\right)$ will more rapidly converge to zero than I_0 does. Therefore, the integrand of the last integral approaches zero as u gets larger. If $I_0(x)$ is approximated as below

$$I_0(x) = \sum_{k=0}^{\infty} \frac{x^{2k}}{2^{2k}(k!)^2} \cong \sum_{k=0}^{N_1} \frac{x^{2k}}{2^{2k}(k!)^2} \quad (41)$$

or $$I_0(Mu) = \sum_{k=0}^{N_1} \frac{M^{2k} u^{2k}}{2^{2k}(k!)^2} \quad \text{where } M = \frac{Z}{\sigma\sqrt{A}}\mu. \quad (42)$$

Then, after some manipulation, I_1 becomes

$$I_1 = \frac{\sigma}{\sqrt{A}\cos\theta} \exp\left[Z^2\left(\frac{1}{2\sigma^2} - \frac{\sigma^2}{2A}\right)\right]\left[\int_0^\infty I_0(Mu)\exp\left(-\frac{u^2}{2}\right)du\right.$$

$$\left. - \frac{\sigma}{\sqrt{A}\cos\theta}\int_0^\infty \frac{1}{u + \frac{\sigma}{\sqrt{A}\cos\theta}} I_0(Mu)\exp\left(-\frac{u^2}{2}\right)du\right] \tag{43}$$

The first part of Eq. (43) is integrated by parts and by use of the approximate expansion for $I_0(x)$ of Eq. (41); this yields

$$I_2 = \int_0^\infty I_0(Mu)\exp\left(-\frac{u^2}{2}\right)du \cong \sum_{k=0}^{N_1}\sqrt{\frac{\pi}{2}}\frac{(2k)!\,M^{2k}}{2^{3k}(k!)^3}$$

$$= \sqrt{\frac{\pi}{2}}\sum_{k=0}^{N_1}\frac{(2k)!\,\mu^{2k}}{2^{3k}(k!)^3\sigma^{2k}A^k}Z^{2k} \tag{44}$$

The second integral of Eq. (43) can be calculated if $\left(\frac{1}{u + \frac{\sigma}{\sqrt{A}\cos\theta}}\right)$ is expanded into Taylor series about $u = \alpha$ as follows,

$$F(x) = \sum_{h=0}^{\infty} F^{(h)}(\alpha)\frac{(x-\alpha)^h}{h!} \tag{45}$$

$$g(u) = \frac{1}{u + \frac{\sigma}{\sqrt{A}\cos\theta}} = \frac{1}{\alpha + \frac{\sigma}{\sqrt{A}\cos\theta}}\sum_{h=0}^{\infty}\left(\frac{\alpha - u}{\alpha + \frac{\sigma}{\sqrt{A}\cos\theta}}\right)^h \tag{46}$$

The convergence condition for the series is

$$\left|\frac{\alpha - u}{\alpha + \frac{\sigma}{\sqrt{A}\cos\theta}}\right| < 1 . \tag{47}$$

Since $\left(\alpha + \frac{\sigma}{\sqrt{A}\cos\theta}\right) > 0$, this condition can be written as

$$-\frac{\sigma}{\sqrt{A}\cos\theta} < u < 2\alpha + \frac{\sigma}{\sqrt{A}\cos\theta}. \tag{48}$$

If β is assumed to be a sufficiently large number, then one part of Eq. (43) becomes

$$\int_0^{\infty} \frac{1}{u + \frac{\sigma}{\sqrt{A}\cos\theta}} I_0(Mu) \exp\left(-\frac{u^2}{2}\right) du$$

$$\cong \int_0^{\beta} \frac{1}{u + \frac{\sigma}{\sqrt{A}\cos\theta}} I_0(Mu) \exp\left(-\frac{u^2}{2}\right) du. \tag{49}$$

Now for the value of α such that $\left(2\alpha + \frac{\sigma}{\sqrt{A}\cos\theta}\right)$ is much greater than the upper limit β in the above integral, the Eq. (46) may be substituted in Eq. (49), and the series will then converge for u in the closed interval $[0, \beta]$. Hence Eq. (49) becomes

$$\frac{1}{\alpha + \frac{\sigma}{\sqrt{A}\cos\theta}} \sum_{h=0}^{N_2} \left(\frac{1}{\alpha + \frac{\sigma}{\sqrt{A}\cos\theta}}\right)^h \int_0^{\beta} (\alpha - u)^h I_0(Mu) \exp\left(-\frac{u^2}{2}\right) du \tag{50}$$

Here again the same approximation is employed for $I_0(Mu)$ in order to reduce the infinite sum to a finite sum up to $h = N_2$, as was done previously. On expanding $(\alpha - u)^h$ by means of binomial expansion and substituting the

result into Eq. (50), it becomes

$$\frac{1}{\alpha+\frac{\sigma}{\sqrt{A}\cos\theta}}\sum_{h=0}^{N_2}\left[\left(\frac{1}{\alpha+\frac{\sigma}{\sqrt{A}\cos\theta}}\right)^h\sum_{i=0}^{h}C_i^h\,\alpha^{h-i}(-1)^i\int_0^{\beta}u^i I_0(Mu)\exp(-\frac{u^2}{2})du\right]\cong$$

$$\frac{1}{\alpha+\frac{\sigma}{\sqrt{A}\cos\theta}}\sum_{2m=0}^{N'_2}\sum_{n=0}^{m}\sum_{k=0}^{N_1}\left(\frac{1}{\alpha+\frac{\sigma}{\sqrt{A}\cos\theta}}\right)^{2m}C_{2n}^{2m}\,\alpha^{2(m-n)}(-1)^{2n}$$

$$\left(\frac{M^{2k}}{2^{2k}(k!)^2}\right)\int_0^{\beta}u^{2(k+n)}\exp(-\frac{u^2}{2})du$$

$$+\frac{1}{\alpha+\frac{\sigma}{\sqrt{A}\cos\theta}}\sum_{2m+1=1}^{N'_2}\sum_{n=0}^{m}\sum_{k=0}^{N_1}\left(\frac{1}{\alpha+\frac{\sigma}{\sqrt{A}\cos\theta}}\right)^{2m+1}C_{2n+1}^{2m+1}\,\alpha^{2(m-n)}(-1)^{2n+1}$$

$$\left(\frac{M^{2k}}{2^{2k}(k!)^2}\right)\int_0^{\beta}u^{2(k+n)+1}\exp(-\frac{u^2}{2})du \qquad (51)$$

After the evaluation of the integrals by parts, Eq. (51) becomes

$$I_3=\frac{\sqrt{\pi/2}}{\alpha+\frac{\sigma}{\sqrt{A}\cos\theta}}\sum_{2m=0}^{N'_2}\sum_{n=0}^{m}\sum_{k=0}^{N_1}\left(\frac{1}{\alpha+\frac{\sigma}{\sqrt{A}\cos\theta}}\right)^{2m}C_{2n}^{2m}\,\alpha^{2(m-n)}$$

$$\frac{\{2(k+n)\}!\,\mu^{2k}}{2^{3k+n}(k!)^2\,(k+n)!\,\sigma^{2k}A^k}\,z^{2k}$$

$$-\frac{\sqrt{\pi/2}}{\alpha+\frac{\sigma}{\sqrt{A}\cos\theta}}\sum_{2m+1=1}^{N'_2}\sum_{n=0}^{m}\sum_{k=0}^{N_1}\left(\frac{1}{\alpha+\frac{\sigma}{\sqrt{A}\cos\theta}}\right)^{2m+1}C_{2n+1}^{2m+1}\,\alpha^{2(m-n)}$$

$$\times \frac{2^n (k+n)!}{2^k (k!)^2} \frac{\mu^{2k}}{\sigma^{2k} A^k} Z^{2k} \tag{52}$$

Equation (36) gives

$$\left[W\right]_{Z'} = 1 - \frac{2}{t_1 + 1} + 2\left(\frac{2}{t_1 + 1} - 1\right) I_1$$

$$= 1 - \frac{2}{t_1 + 1} + 2\left(\frac{2}{t_1 + 1} - 1\right) \frac{\sigma}{\sqrt{A}\cos\theta}$$

$$\exp\left[Z^2\left(\frac{1}{2\sigma^2} - \frac{\sigma^2}{2A}\right)\right] \left(I_2 - \frac{\sigma}{\sqrt{A}\cos\theta} I_3\right) \tag{53}$$

The following notation is employed in order to simplify calculation;

$$I_2 = D_1 Z^{2k} \tag{54}$$

$$\frac{\sigma}{\sqrt{A}\cos\theta} I_3 = D_2 Z^{2k} - D_3 Z^{2k} = (D_2 - D_3) Z^{2k} \tag{55}$$

where D_1, D_2 and D_3 are appropriate factors in Eqs. (44) and (52).

Next, $\left[W\right]_{Z'}$ is averaged over Z using its Rayleigh probability density.

$$q(Z) = \frac{Z}{\sigma^2} \exp\left(-\frac{Z^2}{2\sigma^2}\right), \quad Z \geqq 0,$$

$$\left[W\right]_Z = \int_0^\infty \left[W\right]_{Z'} q(Z)\, dZ$$

$$= 1 - \frac{2}{\sigma^2} \int_0^\infty \frac{Z}{t_1 + 1} \exp\left(-\frac{Z^2}{2\sigma^2}\right) dZ$$

$$+ \frac{4}{\sigma\sqrt{A}\cos\theta} (D_1 - D_2 + D_3) \int_0^\infty \frac{Z^{2k+1}}{t_1 + 1} \exp\left(-\frac{\sigma^2}{2A} Z^2\right) dZ$$

$$-\frac{2}{\sigma\sqrt{A}\cos\theta}(D_1 - D_2 + D_3)\int_0^\infty Z^{2k+1}\exp(-\frac{\sigma^2}{2A}Z^2)dZ \qquad (56)$$

Let I_4, I_5 and I_6 denote the first, second, and third integral in Eq. (56). Now simplifying I_4, it becomes

$$I_4 = \int_0^\infty \frac{Z}{t_1 + 1}\exp(-\frac{Z^2}{2\sigma^2})dZ$$

$$= \frac{1}{\cos\theta}\int_0^\infty \exp(-\frac{Z^2}{2\sigma^2})dZ - \frac{1}{\cos^2\theta}\int_0^\infty \frac{1}{Z+1/\cos\theta}\exp(-\frac{Z^2}{2\sigma^2})dZ$$

$$\cong \frac{\sigma}{\cos\theta}\sqrt{\frac{\pi}{2}} - \frac{1}{\cos^2\theta}\left(\frac{1}{\alpha + 1/\cos\theta}\right)\sum_{h=0}^{n}\left(\frac{1}{\alpha + \frac{1}{\cos\theta}}\right)^h$$

$$\int_0^\nu (\alpha - Z)^h \exp(-\frac{Z^2}{2\sigma^2})dZ \qquad (57)$$

In order to obtain the last expression, the expansion similar to Eq. (44) is used. The expression $\left[2\alpha + (1/\cos\theta)\right]$ is assumed to be larger than ν. After lengthy evaluation I_4 can be expressed as

$$I_4 \cong \frac{\sigma}{\cos\theta}\sqrt{\frac{\pi}{2}} - \frac{1}{\cos\theta}\left(\frac{1}{\alpha\cos\theta+1}\right)\sum_{\substack{2m\\=0}}^{n'}\sum_{j=0}^{m}\left(\frac{1}{\alpha + \frac{1}{\cos\theta}}\right)^{2m}$$

$$C_{2j}^{2m}\,\alpha^{2(m-j)}\,\frac{\sigma^{2j+1}(2j)!}{2^j\, j!}\sqrt{\frac{\pi}{2}}$$

$$+\frac{1}{\cos\theta}\left(\frac{1}{\alpha\cos\theta+1}\right)\sum_{\substack{2m+1\\=1}}^{n''}\sum_{j=0}^{m}\left(\frac{1}{\alpha+\frac{1}{\cos\theta}}\right)^{2m+1}C_{2j+1}^{2m+1}\,\alpha^{2(m-j)}\,\sigma^{-2j+2}2^{j}j! \tag{58}$$

Similarly in $I_5 = \int_0^{\infty}\frac{Z^{2k+1}}{t_1+1}\exp(-\frac{\sigma^2}{2A}Z^2)dZ$, the expression $\frac{Z^{2k+1}}{t_1+1}$ may be expanded as follows:

$$\frac{Z^{2k+1}}{t_1+1}\cong\frac{1}{\alpha\cos\theta+1}\sum_{h=0}^{n}\left(\frac{\alpha-Z}{\alpha+\frac{1}{\cos\theta}}\right)^{h}Z^{2k+1}$$

$$=\frac{1}{\alpha\cos\theta+1}\sum_{h=0}^{n}\left(\frac{1}{\alpha+\frac{1}{\cos\theta}}\right)^{h}\sum_{i=0}^{h}C_i^h\,\alpha^{h-i}(-1)^i\,Z^{2k+i+1} \tag{59}$$

Using this result I_5 becomes,

$$I_5\cong\int_0^{\delta}\frac{1}{\alpha\cos\theta+1}\sum_{h=0}^{n}\sum_{i=0}^{h}\left(\frac{1}{\alpha+\frac{1}{\cos\theta}}\right)^{h}C_i^h\,\alpha^{h-i}(-1)^i\,Z^{2k+i+1}$$

$$\exp(-\frac{\sigma^2}{2A}Z^2)dZ$$

$$\cong\frac{1}{\alpha\cos\theta+1}\sum_{\substack{2p\\=0}}^{n'}\sum_{j=0}^{p}\left(\frac{1}{\alpha+\frac{1}{\cos\theta}}\right)^{2p}C_{2j}^{2p}\,\alpha^{2(p-j)}\left(\frac{\sqrt{A}}{\sigma}\right)^{2(k+j+1)}2^{k+j}(k+j)!$$

$$-\frac{1}{\alpha\cos\theta+1}\sum_{\substack{2p+1\\=1}}^{n''}\sum_{j=0}^{p}\left(\frac{1}{\alpha+\frac{1}{\cos\theta}}\right)^{2p+1}C_{2j+1}^{2p+1}\,\alpha^{2(p-j)}\left(\frac{\sqrt{A}}{\sigma}\right)^{2(k+j)+3}$$

$$\frac{(2k+2j+2)!}{2^{k+j+1}(k+j+1)!}\sqrt{\frac{\pi}{2}} \tag{60}$$

$$I_6 = \int_0^\infty Z^{2k+1} \exp(-\frac{\sigma^2}{2A} Z^2) dZ = (\frac{\sqrt{A}}{\sigma})^{2k+2} 2^k(k!) \qquad (61)$$

Since $$\left[W\right]_Z = 1 - \frac{2}{\sigma^2} I_4 + \frac{4}{\sigma\sqrt{A}\cos\theta} (D_1 - D_2 + D_3) I_5$$

$$- \frac{2}{\sigma\sqrt{A}\cos\theta} (D_1 - D_2 + D_3) I_6 ,$$

the substitution of Eqs. (58), (60) and (61) into the above relation results in the final expression for $\left[W\right]_Z$.

$$\left[W\right]_Z = 1 - \frac{\sqrt{2\pi}}{\sigma\cos\theta} + \frac{1}{\cos\theta} (\frac{1}{\alpha\cos\theta + 1}) \sum_{\substack{2m \\ =0}}^{n'} \sum_{j=0}^{m} (\frac{1}{\alpha + \frac{1}{\cos\theta}})^{2m} C_{2j}^{2m} \alpha^{2(m-j)}$$

$$\frac{\sigma^{2j-1} (2j)!}{2^{j-1} j!} \sqrt{\frac{\pi}{2}}$$

$$- \frac{1}{\cos\theta} (\frac{1}{\alpha\cos\theta + 1}) \sum_{\substack{2m+1 \\ =1}}^{n''} \sum_{j=0}^{m} (\frac{1}{\alpha + \frac{1}{\cos\theta}})^{2m+1} C_{2j+1}^{2m+1} \alpha^{2(m-j)}$$

$$\sigma^{2j} 2^{j+1} j!$$

$$+ \frac{4}{\sigma\sqrt{A}\cos\theta} (D_1 - D_2 + D_3) \frac{1}{\alpha\cos\theta + 1} \sum_{2p=0}^{n'} \sum_{j=0}^{p} (\frac{1}{\alpha + \frac{1}{\cos\theta}})^{2p}$$

$$C_{2j}^{2p} \alpha^{2(p-j)} (\frac{\sqrt{A}}{\sigma})^{2(k+j+1)} 2^{k+j} (k+j)!$$

$$- \frac{4}{\sigma\sqrt{A}\cos\theta} (D_1 - D_2 + D_3) \frac{1}{\alpha\cos\theta + 1} \sum_{\substack{2p+1 \\ =1}}^{n''} \sum_{j=0}^{p} \left(\frac{1}{\alpha + \frac{1}{\cos\theta}}\right)^{2p+1}$$

$$C_{2j+1}^{2p+1} \alpha^{2(p-j)} \left(\frac{\sqrt{A}}{\sigma}\right)^{2(k+j)+3} \frac{(2k+2j+2)!}{2^{(k+j+1)}(k+j+1)!} \sqrt{\frac{\pi}{2}}$$

$$- \frac{2}{\sigma\sqrt{A}\cos\theta} (D_1 - D_2 + D_3) \left(\frac{\sqrt{A}}{\sigma}\right)^{2k+2} 2^k\, k! \,, \tag{62}$$

where $$D_1 = \sqrt{\frac{\pi}{2}} \sum_{k=0}^{N_1} \frac{(2k)!\, \mu^{2k}}{2^{3k} (k!)^3 \sigma^{2k} A^k} \,, \tag{63}$$

$$D_2 = \sqrt{\frac{\pi}{2}} \frac{\frac{\sigma}{\sqrt{A}\cos\theta}}{\alpha + \frac{\sigma}{\sqrt{A}\cos\theta}} \sum_{\substack{2m \\ =0}}^{N_2'} \sum_{n=0}^{m} \sum_{k=0}^{N_1} \left(\frac{1}{\alpha + \frac{\sigma}{\sqrt{A}\cos\theta}}\right)^{2m} C_{2n}^{2m} \alpha^{2(m-n)}$$

$$\frac{\{2(k+n)\}!\, \mu^{2k}}{2^{3k+n} (k!)^2 (k+n)!\, \sigma^{2k} A^k} \,, \tag{64}$$

$$D_3 = \sqrt{\frac{\pi}{2}} \frac{\frac{\sigma}{\sqrt{A}\cos\theta}}{\alpha + \frac{\sigma}{\sqrt{A}\cos\theta}} \sum_{\substack{2m+1 \\ =1}}^{N_2''} \sum_{n=0}^{m} \sum_{k=0}^{N_1} \left(\frac{1}{\alpha + \frac{\sigma}{\sqrt{A}\cos\theta}}\right)^{2m+1} C_{2n+1}^{2m+1}$$

$$\alpha^{2(m-n)} \frac{2^n (k+n)!\, \mu^{2k}}{2^k (k!)^2 \sigma^{2k} A^k} \,. \tag{65}$$

Substitution of Eq. (62) in Eq. (30) results in the expression for the average received power:

$$\overline{P}_r = \frac{P_T G^2}{32\pi^2} R_e \iiiint \frac{\cot\theta \cdot \cot\theta'}{R\, R'} \left[W\right]_Z \exp\left[-j2k(R - R')\right]$$

$$dR\, dR'\, d\psi\, d\psi' \,. \tag{66}$$

Extension to Complex Impedance Case*

Calculations in the previous section can be extended to random complex impedance variation case, because in reality, the randomly varying heights cause both amplitude and phase attenuation, and these may be appropriately represented by an equivalent complex impedance.

First, Z's in the expressions for I_4, I_5 and I_6 should be replaced by $aZ = R + j\,X$ where $a = \exp(j\alpha)$. aZ represents a complex impedance. Next these integrals will be averaged over α using its uniform density function for $0 < \alpha < 2\pi$, as

$$I_4 = \int_0^{2\pi}\int_0^{\infty} \frac{aZ}{aZ\cos\theta + 1} \exp\left(-\frac{Z^2}{2\sigma^2}\right) \frac{1}{2\pi}\, dZ\, d\alpha \qquad (67)$$

$$I_5 = \int_0^{2\pi}\int_0^{\infty} \frac{(a\,Z)^{2k+1}}{aZ\cos\theta + 1} \exp\left(-\frac{\sigma^2}{2A} Z^2\right) \frac{1}{2\pi}\, dZ\, d\alpha \qquad (68)$$

$$I_6 = \int_0^{2\pi}\int_0^{\infty} (a\,Z)^{2k+1} \exp\left(-\frac{\sigma^2}{2A} Z^2\right) \frac{1}{2\pi}\, dZ\, d\alpha\,. \qquad (69)$$

Substitution of new I_4, I_5 and I_6 into the expression (56) for $[W]_Z$ gives a new reflection coefficient which accounts of the complex impedance variation.

As it is clear from the simple geometry of Figure 1B, the magnitude of impedance can be approximated as βZ where $\beta = 1 + \frac{R_0}{R - R_0}$

and $R_0 = X_0$ (assumed), (70)

---

* The material on pages 19 through 21 is included at the request of the Major Professor and is not concurred in by members of the committee in the Electrical Engineering Department.

R is a real component of the impedance and R_0 is its mean value. Since $R_1 = R - R_0$ and $X_1 = X - X_0$ have normal probability density of the form

$$p(R_1) = \frac{1}{\sqrt{2\pi\sigma^2}} \exp\left(-\frac{R_1^2}{2\sigma^2}\right), \tag{71}$$

a probability density $p_1(\beta)$ for the quantity β can be expressed as

$$p_1(\beta) = \frac{p(R)}{\left|\frac{\partial\beta}{\partial R_1}\right|} = \frac{R_1^2}{\sqrt{2\pi\sigma^2 R_0^2}} \exp\left(-\frac{R_1^2}{2\sigma^2}\right). \tag{72}$$

Then, $$\int_1^\infty \beta [W]_Z \, p_1(\beta) \, d\beta \tag{73}$$

gives the final value of the reflection coefficient function, $[W]_Z$.

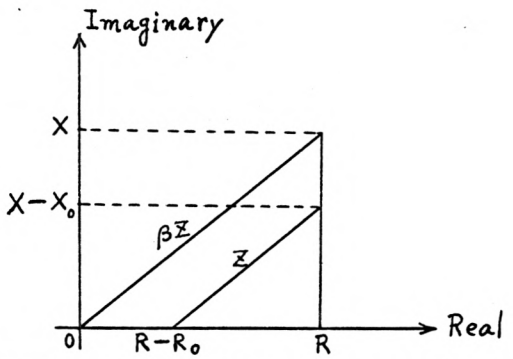

Figure 1B. Geometry of impedance

This is a crude approximation based on the fact that R_0 and X_0 are equal but an exact solution is discussed in the following paragraph.

First of all the equivalent surface impedance must be angle of incidence dependent but this makes the problem far more complex, and hence this approach is not followed. Secondly the real R and imaginary X components of Z are

assumed to be independent and noramlly distributed with (R_0, σ_R) and (X_0, σ_X) respectively. Furthermore, it is assumed that $\sigma_R = \sigma_X = \sigma$, and X_0 may or may not be equal to R_0. Then the probability density function of Z is obtained as follows:

$$p(R) = \frac{1}{\sqrt{2\pi\sigma^2}} \exp\left[-\frac{(R-R_0)^2}{2\sigma^2}\right], \quad -\infty < R < +\infty \tag{74}$$

$$p(X) = \frac{1}{\sqrt{2\pi\sigma^2}} \exp\left[-\frac{(X-X_0)^2}{2\sigma^2}\right], \quad -\infty < x < +\infty \tag{75}$$

and $$p(Z, \alpha)dZ\, d\alpha = p(R, X)dR\, dX, \tag{76}$$

where $$p(R, X) = p(R)\, p(X), \tag{77}$$

and $$dR\, dX = Z\, dZ\, d\alpha. \tag{78}$$

Hence, $$p(Z, \alpha) = \frac{Z}{2\pi\sigma^2} \exp\left[-\frac{(R - R_0)^2 + (X - X_0)^2}{2\sigma^2}\right] \tag{79}$$

where $R = Z \cos\alpha$

$X = Z \sin\alpha$.

Then, the quantity W should be integrated over Z, Z' and α, using a modified conditional density function $f(Z' / Z, \vec{r})$ which can be derived in the same way as Eq. (35).

Conclusions

The quantity $\left[W\right]_Z$ has dimension of the square of reflection coefficient and varies with θ, σ, and μ, which are the angle of incidence, standard deviation, and autocorrelation function respectively.

A proper assumption of the form of autocorrelation function will be needed before a reduced final expression for the average received power is

obtained. The radiation from a particular small area on the terrain was assumed to be isotropic, without which this problem would be quite complex. There will be no significant error due to the assumption of isotropic radiation, as it can be intuitively justified from wave optic reflection mechanism.

The reflection of a plane wave from the terrain with randomly varying equivalent impedance cannot be calculated using classical theory of geometrical optics, and therefore the use of statistical theory is necessary.

AN ELECTRONIC SAMPLER FOR THE ACOUSTIC SIMULATION FACILITY

In an acoustic simulator, shown in Figure 2A, the sound waves of a particular frequency are used to simulate the electromagnetic wave in radar systems. A pulsed oscillator generates a carrier frequency ranging from 10 kc to 25 mc either in a pulse or continuous wave (cw) form. This signal is converted into an acoustic wave by the transducer A, and the resulting wave travels through water and eventually becomes incident on the target surface. Since the target surface roughness can be described statistically, the reflected wave contains sufficient information about the surface roughness in its amplitude and phase variations.

The reflected acoustic wave is converted into an electric signal by the acoustic-electro-transducer B. The signal is envelope-detected and amplified. Then it is necessary to sample the envelope for statistical analysis in order to obtain an estimate of target surface roughness.

Sampling can be accomplished either manually or electronically. This part describes an electronic sampler which will perform the sampling task.

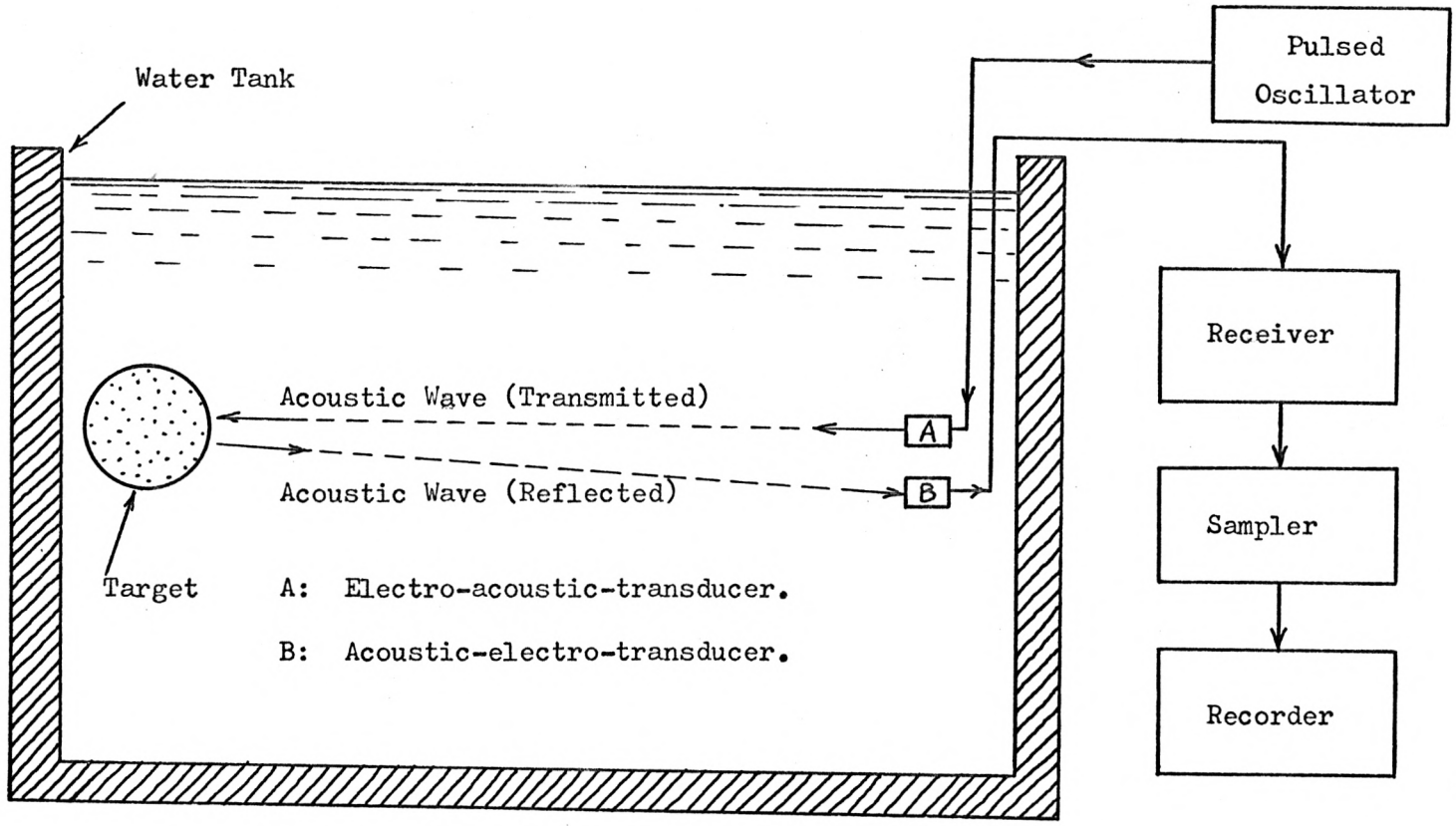

Figure 2A. The Acoustic Simulator System for Radar Return.

Design Criterion

The output envelope waveform in the case of pulsed operation has been specified as below by previous experimentation (Hayre, 1962).

(1) The highest frequency component of interest is 20 kc.

(2) Maximum pulse width, τ_{max}, is approximately 100 microseconds.

(3) Pulse repetition frequency is 3 kc.

(4) Amplitude varies from zero to a maximum of + 25 mV. The sampler is required to process such pulses with the following constraints.

1. The first sample (at t_1) should be at 1 to 3 microseconds from the start of the signal.

2. Each pulse must be sampled at six or fewer equally spaced points as shown in Figure 2B. These six sampled pulses per each original pulse are to be separated on time basis by a time-division multiplex circuit which will be placed between the sampler and the recorder.

3. The desired output level is to be of the order of a few volts.

Circuit Diagram

A block diagram of such a system is shown in Figure 3. The wave-front of input pulse must first be detected, and consequently a sampling pulse must be generated.

An input amplifier, a Schmitt circuit and a multi-vibrator connected in cascade would realize the desired objectives. For instance, if an input pulse arrives, the Schmitt circuit produces a square wave whose duration is made as nearly equal to that of the input signal as possible. The time delay which exists is determined by a steepness of front edge of input pulse to the first Schmitt trigger and is reduced by use of the input amplifier.

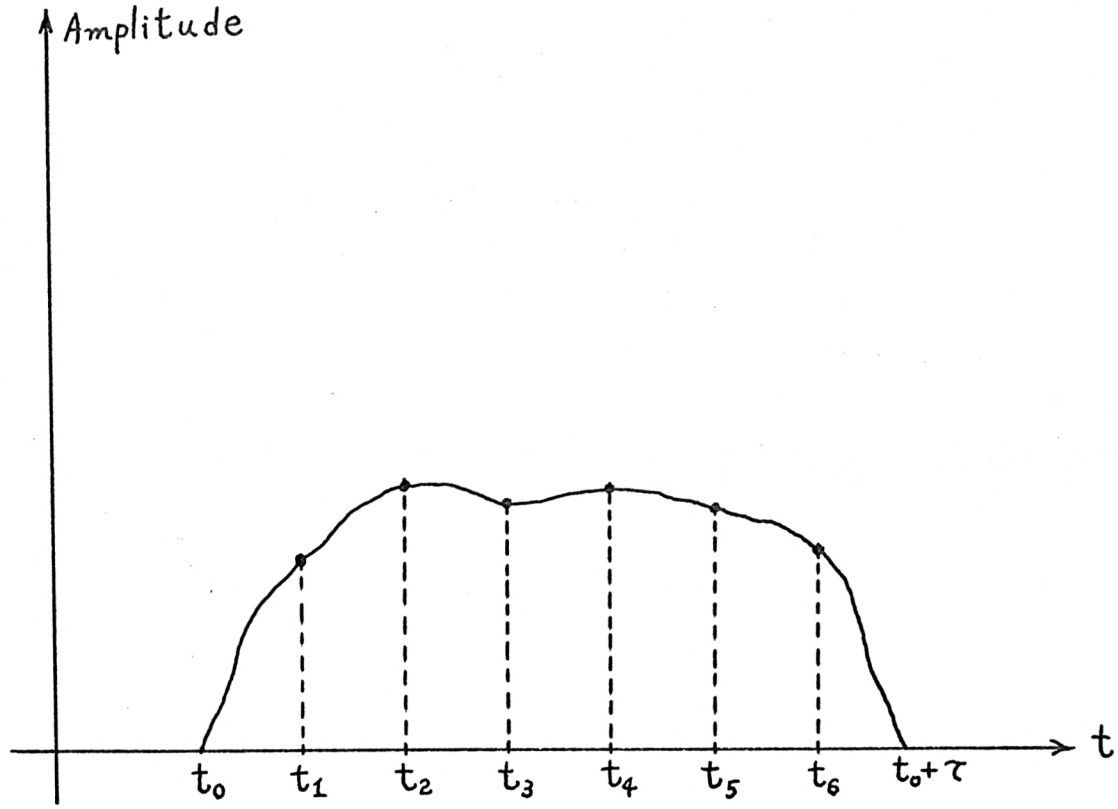

Figure 2B. Input Pulse Envelope and Sample Points.

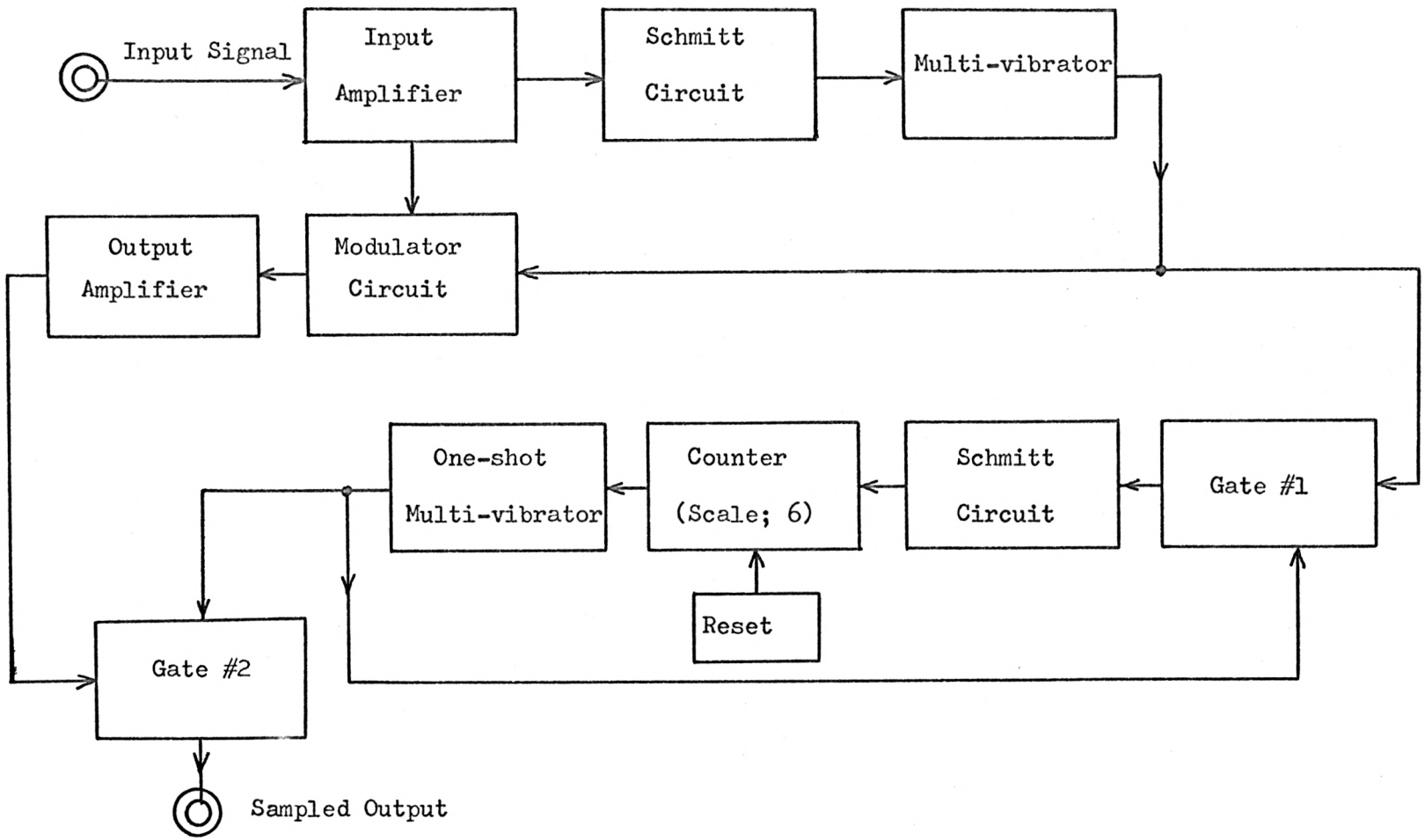

Figure 3. Block Diagram of the Sampler.

The multi-vibrator is controlled by the square wave, and it continues to produce sampling pulses as long as the positive square wave maintains the multi-vibrator out of cut-off region. The output pulses of the multi-vibrator are amplitude-modulated by the input signal in a modulator circuit. These amplitude modulated pulses represent exactly the sampled values of the input signal with a sampling interval equal to the period of output pulses of the multi-vibrator. The modulated pulses are then amplified by the output amplifier and are passed to gate #2 which is normally open.

A part of the output of the multi-vibrator goes to a normally open gate #1 in order to trigger the Schmitt circuit whose output is applied to a counter with a scale of six. The counter is designed to receive six negative pulses before producing an output pulse. It is provided with a reset circuit to correct any miscounting. One-shot multi-vibrator which follows the counter produces a negative square wave with a prescribed time duration when triggered by the counter output pulse. The negative square wave in turn closes both gates so as to block the incoming pulses during the presence of the control signal. Consequently, as soon as the counter finishes counting six, the closing of both gates blocks the sampled pulses number seven and higher, and likewise no more than six trigger pulses will be applied to the counter for each input pulse. The system described above is realized using the circuits of Figure 4. This system was built, tested, and the resulting corrections are incorporated in Figure 4.

Analysis of the Actual Circuits

Some detailed discussion and analysis of the actual circuits will be given.

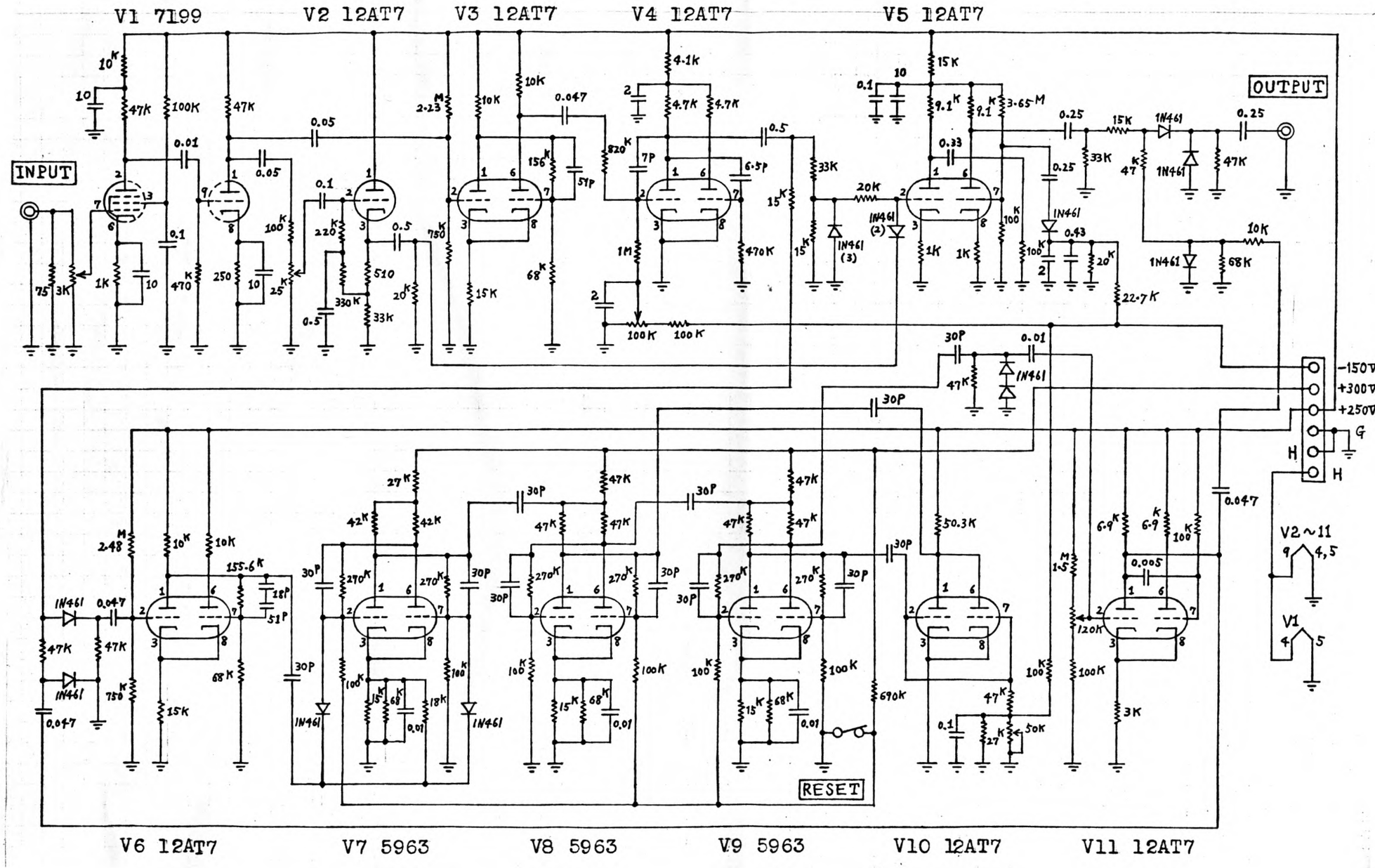

Figure 4. Schematic Diagram of the Sampler.

1. The Input Amplifier (V1; 7199)

The input amplifier is essentially a pulse amplifier for 3 kc square wave, and its response can be specified by its percentage tilt and rise time. The time constants of cathode and screen grid circuits are chosen to be sufficiently large for the input signal frequency. Hence, the rise time and percentage tilt are affected by coupling networks and input capacitances of the tubes only. The percentage tilt due to the first coupling network composed of C_{c1} and R_{g1} is calculated.

$$P_1 = 100\,\pi \times \frac{f_2}{f} \cong 3.3\ (\%), \tag{80}$$

where $f_2 = \dfrac{1}{2\pi R_{g1} C_{c1}}$, $f = 3000$ cps,

$R_{g1} = 470\ k\Omega$, $C_{c1} = 0.01\ \mu F$,

whereas that due to the second coupling network, (C_{c2}, R_{g2}) is

$$P_2 = 100\,\pi \times \left(\frac{1}{3000} \times \frac{1}{2\pi R_{g2} C_{c2}}\right) \tag{81}$$

$$\cong 0.6\ (\%).$$

The percentage tilt for PRF of 3 kc will be less than 1/1.6 of the calculated values. The rise time of the first stage t_{r1} is

$$t_{r1} = 2.2\ R\ C \tag{82}$$

$$= 2.2 \times 47 \times 10^3 \times 30 \times 10^{-12} = 3.1 \times 10^{-6}$$

$$= 3.1\ \mu \text{ Sec.}$$

where $R \cong R_{L1} = 47\ K\Omega$, $C = C_{\text{out 1}} + C_{\text{in 1}} + C_{gp1}\,(1+A) \cong 30\ pF$

A is a gain of the second triode stage, whereas that of the second stage t_{r2} is

$$t_{r2} = 2.2 \times R_2 \times \left\{ C\,out_2 + C\,in_2 + C_{gp2}\,(1+A') \right\}$$

$$= 2.2 \times 47 \times 10^{3} \times 25 \times 10^{-12} = 2.5\ \mu\ \text{Sec.}$$

where A' is a gain of V2. The total rise time t_r can be expressed as

$$t_r = \sqrt{t_{r1}^2 + t_{r2}^2} = \sqrt{3.1^2 + 2.5^2} \times 10^{-6} \cong 4\ \mu\ \text{Sec.} \qquad (83)$$

The static operating conditions of the pentode and triode stages of the amplifier are summarized below.

(i) Pentode stage

plate supply voltage = 205 volts

zero signal plate voltage = 75 volts

zero signal plate current = 3.2 mA

zero signal screen grid voltage = 150 volts

zero signal screen grid current = 1.3 mA

cathode voltage = 3 volts

gain (at midband) = 36 db

(ii) Triode stage

plate supply voltage = 250 V

zero signal plate voltage = 50 volts

zero signal plate current = 3.7 mA

cathode voltage = 1.0 volt

gain (at midband) = 23 db

(iii) Total gain (at midband) = 59 db

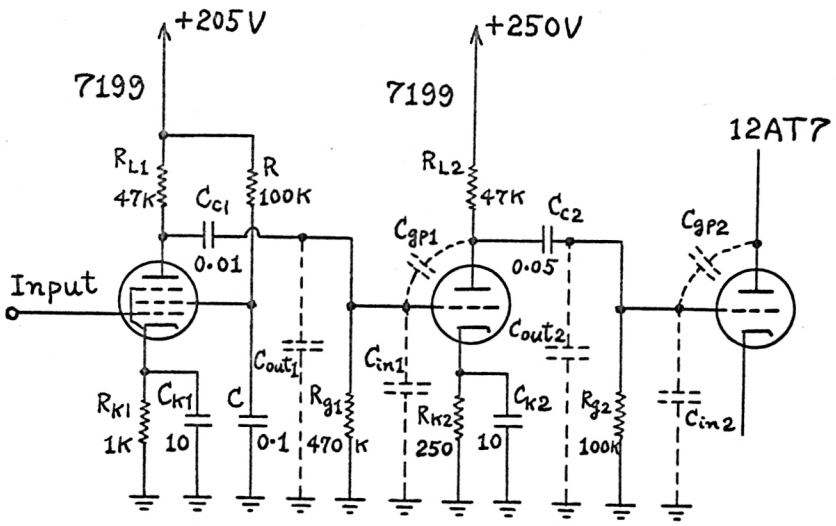

Figure 5. The Input Amplifier Where Stray Capacitances are Shown.

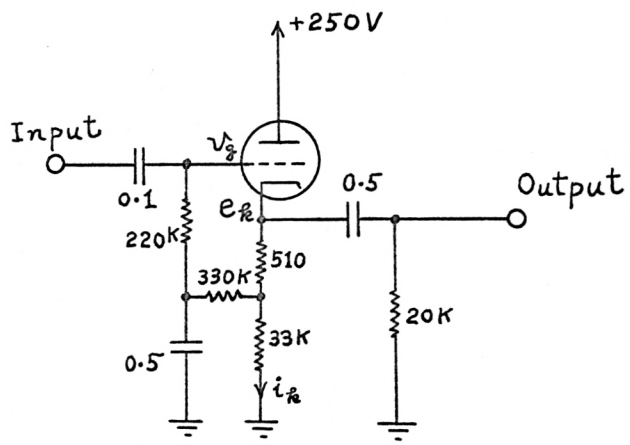

Figure 6. Cathode Follower Circuit.

2. Input Cathode Follower (V2; 12AT7)

A cathode follower is employed to provide the modulating signal with a low source impedance to the modulator. The quiescent operating point is defined by

$$i_k = 3.25 \text{ mA}$$

$$e_k = 109 \text{ volts}$$

$$V_{gk} = -1.65 \text{ volts}$$

and its gain is

$$A \cong \frac{g_m r_k}{1 + g_m r_k} = \frac{(2.5 \times 10^{-3}) \times (12 \times 10^3)}{1 + (2.5 \times 10^{-3}) \times (12 \times 10^3)} = \frac{30}{31} \cong 0.97$$

where r_k is ac circuit resistance between the cathode and the ground. Its output impedance is given by

$$R_o \cong \frac{1}{1/r_k + g_m} = \frac{1}{1/(12 \times 10^3) + 2.5 \times 10^{-3}} \cong 390 \text{ ohms.}$$

Time constants of coupling networks and bypassing network are so chosen that the input signal is not distorted by this amplifier.

3. The Schmitt Circuit (V3; 12AT7)

For v = 0 in Figure 7, the potential at P_1 is essentially 250 volts. The attenuator ratio $a = \frac{R_2}{R_1 + R_2}$ is so selected that the grid-to-cathode voltage of T_2 is -1 volt. It may then be verified from the tube characteristics that i_2 = 5 mA and therefore cathode voltage is 75 volts and hence T_1 is indeed cut off. The voltage at G_2 is 75 - 1 = 74 volts and $a = \frac{74}{250} = 0.30$.

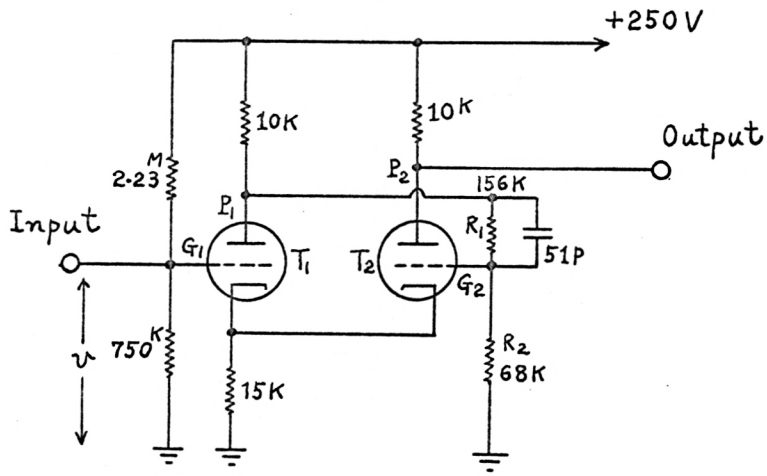

Figure 7. The Schmitt Circuit.

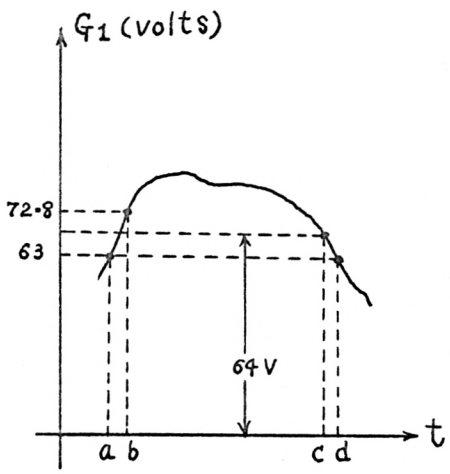

Figure 8. Input Signal Superposed on the dc-bias

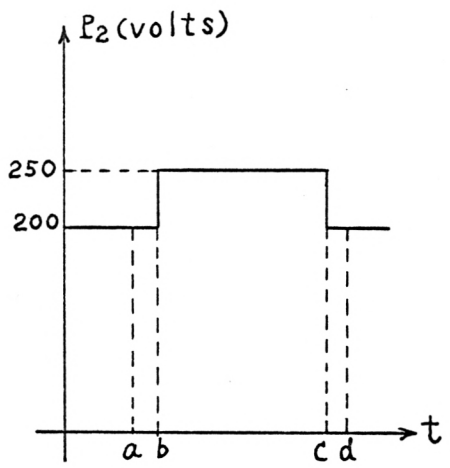

Figure 9. Output Square Wave from P_2

Now, as the input voltage v is increased, the circuit will not respond until T_1 comes out of cut-off. Note that the plate-to-cathode drop of T_1 is 250-75 = 175 volts, for which cut-off occurs at a bias of -2.2 volts. Hence, when v = -2.2 + 75 = 72.8 volts, T_1 starts to conduct. Then P_1 and G_2 potential will drop. The signal at G_2 is transferred to T_1 through the cathode circuit and reappears at P_1 with the same polarity as at G_2. The signal at P_1 is now transferred again to G_2, and if the loop gain exceeds unity a regenerative action will take place driving T_2 to cut-off. Assuming then that T_2 is cut-off and v = 72.8 volts, i_1 is found to be approximately 4.92 mA. The voltage at G_2 is (250 - 4.92 x 10) x a = 60.24 volts, while the cathode voltage is 4.92 x 15 = 73.9. The grid-to-cathode voltage of T_2 is 60.2 - 73.9 = -13.7 volts, which verifies that T_2 is cut off. The output signal from P_2 consists of a positive step of amplitude $i_2 R_L$ = 50 volts. After the circuit has been triggered, further increase in v has no effect on the voltage at P_2. This circuits exhibits hysteresis or in other words, the value of voltage at which triggering occurs depends upon whether v is increasing or decreasing. However, this hysteresis does not have any undesirable effect on the present usage of the circuit. Typical wave-forms of input and output signal are illustrated in Figure 8 and Figure 9.

4. The Multi-vibrator (V4; 12AT7)

When the output voltage v_{in} keeps T_1 out of cut off, the equivalent circuit of the multi-vibrator Figure 10 can be reduced as shown in Figures 11, 12 and 13.

From Figure 13 (b), E_{R1} is

$$E_{R1} = -\left(E_{bb}\frac{R_{L2}}{R_{b2}+R_{L2}}\right)\left(\frac{R_1}{R'_1}\right)\exp\left(-\frac{t}{C_1 R'_1}\right)$$

$$= -k_2 E_{bb}\exp(-\alpha_1 t), \tag{84}$$

where $k_2 = \left(\frac{1}{1+\frac{R_{b2}}{R_{L2}}}\right)\left\{\frac{1}{1+\frac{1}{R_1}\left(\frac{R_{b2}\,R_{L2}}{R_{b2}+R_{L2}}\right)}\right\}$ (85)

and $R'_1 = R_1 + \frac{R_{b2}\,R_{L2}}{R_{b2}+R_{L2}}$ (86)

and $\alpha_1 = \frac{1}{C_1 R'_1}$. (87)

When T_1 is first driven into cutoff (t=0), its grid voltage is equal to $-k_2 E_{bb}$. As time elapses, the grid voltage increases exponentially toward zero. When E_{R1} reaches the cutoff value $(-E_{col})$, the tube begins to conduct. Now, Eq. (84) can be written as

$$\frac{E_{R1}}{-k_2 E_{bb}} = \exp(-\alpha_1 t). \tag{88}$$

Substituting the specific values $(-E_{col})$ for E_{R1} and τ_1 for t, Eq. (88) becomes

$$\frac{E_{col}}{k_2 E_{bb}} = \exp(-\alpha_1 \tau_1),$$

or $$\tau_1 = -\frac{1}{\alpha_1}\ln\left(\frac{E_{col}}{k_2 E_{bb}}\right). \tag{89}$$

$k_2 E_{bb}$ must be greater than E_{col} and therefore, a minimum value for E_{bb} is fixed at E_{col}/k_2. The portion T_2 of the multi-vibrator is calculated by using Eq. (90).

$$\tau_2 = -\frac{1}{\alpha_2}\ln\left(\frac{E_{co2}}{k_1 E_{bb}}\right) \tag{90}$$

The period of the multi-vibrator is then expressed as the sum of τ_1 and τ_2.

$$\tau = \tau_1 + \tau_2 \qquad (91)$$

In the present case $\tau_1 = \tau_2$, and $\alpha_1 = \alpha_2$, $k_1 = k_2$, $E_{co1} = E_{co2}$, and therefore τ is calculated as shown below.

E_{bb} = 200 volts, R_L = 4.7 kΩ , R_b = 10 kΩ ,

R_1 = 470kΩ , C_1 = 6.5 pf, E_{co} = 5.0 volts.

$$k = \left(\frac{1}{1 + \frac{10}{4.7}}\right) \frac{1}{1 + \frac{1}{470}\left(\frac{10 \times 4.7}{10 + 4.7}\right)} \cong 0.32$$

$$k E_{bb} = 64 \text{ volts.}$$

$$1/\alpha = 6.5 \times 10^{-12} \left(4.7 \times 10^5 + \frac{10 \times 4.7}{10 + 4.7} \times 10^3\right) \cong 3.07 \times 10^{-6}$$

$$\tau = -\frac{2}{\alpha} \ln\left(\frac{E_{co}}{K E_{bb}}\right) = -6.14 \times 10^{-6} \ln\left(\frac{5.0}{64}\right) \cong 15.7 \times 10^{-6}$$

$$= 15.7 \ \mu \text{ Sec.}$$

However, the actual period of the multi-vibrator is less than the calculated value, and its numerical value is approximately 10 microseconds. This discrepancy is presumably caused by the loading of the plate circuit by input impedances of the following stages and stray capacitances at both grids and these attenuate the plate voltage swing. From the tube characteristics when the grid is clamped at 0 volt, the plate current i_p = 13 mA. Hence, output swing is

13 m A x 4.7 KΩ $\cong$ 60 volts.

The wave-forms at P_1 and G_1 are shown in Figures 14 and 15 respectively.

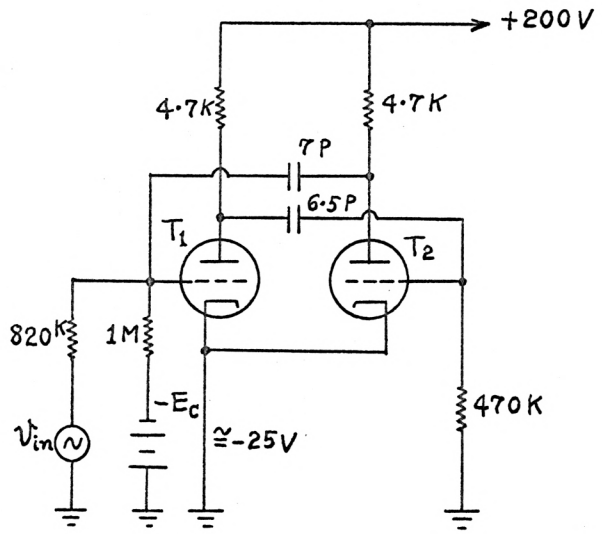

Figure 10. The Multi-vibrator Circuit.

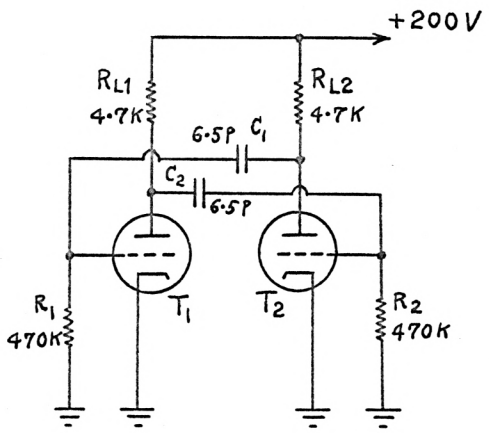

Figure 11. The Equivalent Multi-vibrator Circuit.

Time is measured from the instant T_2 becomes conducting.

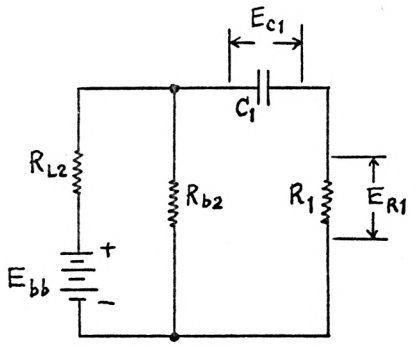

T_2 is on, T_1 is off.

$E_{c1} = E_{bb}$ at t = 0.

Figure 12. Equivalent Discharge Circuit of C_1.

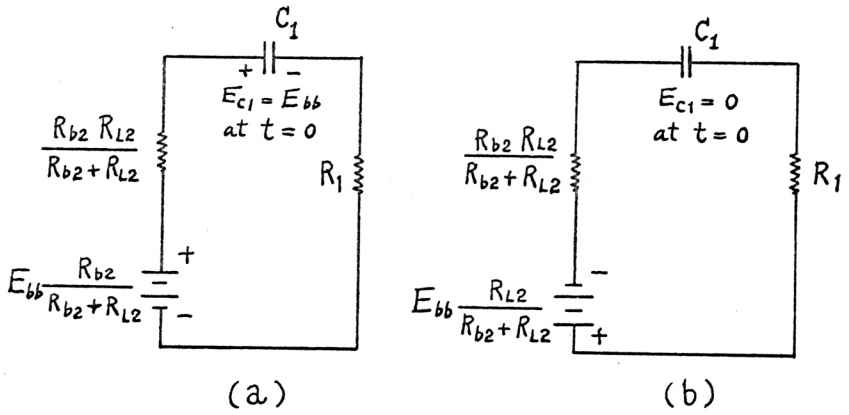

R_{b2} = static plate resistance of T_2.

Figure 13. Simplification of Fig. 12 by the Use of Thevenin's Theorem.

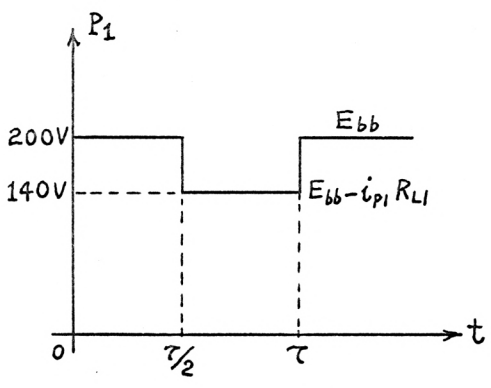

Figure 14. Waveform at P_1 (Calculated)

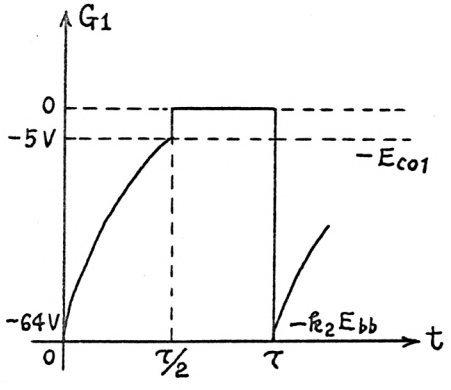

Figure 15. Waveform at G_1 (Calculated)

5. The Modulator Circuit.

The modulator circuit shown in Figure 16 can be redrawn as the equivalent circuit shown in Figure 17.

In Figure 17, R_f and R_r stand for forward and inverse diode resistances respectively, and V'_{in} represents the sampling pulse voltage from the preceding multi-vibrator. V_s is the signal voltage taken from the input amplifier.

In the present case $V'_{in} > V_s > 0$ and $R_r \gg R_f$, so the diode may be replaced by its forward resistance and the output voltage may be written as

$$V_o = \frac{R_1}{R_1 + R_f + R_2} V_s + \frac{R_f + R_2}{R_1 + R_f + R_2} V'_{in} . \qquad (92)$$

Rewriting Eq. (92), it becomes

$$V_o = \frac{R_1}{R_1 + R_f + R_2} V_s \left(1 + \frac{R_f + R_2}{R_1} \frac{V'_{in}}{V_s}\right) . \qquad (93)$$

The term inside the parenthesis in Eq. (93) represents the desired output plus a proportional error term. The error in the equation includes the ratio of the signal producing the undesired transmission to the signal producing the desired transmission. Actually the duration of V_s is slightly longer than that of V'_{in} and the following undesirable situation occurs.

$$V'_{in} = 0 \text{ and } V_s > 0$$

In this case V_o may be expressed as

$$V_o = \frac{R_1}{R_1 + R_r + R_2} V_s \qquad (94)$$

However, since $R_r \gg R_1$, the magnitude of this undesired output is negligible.

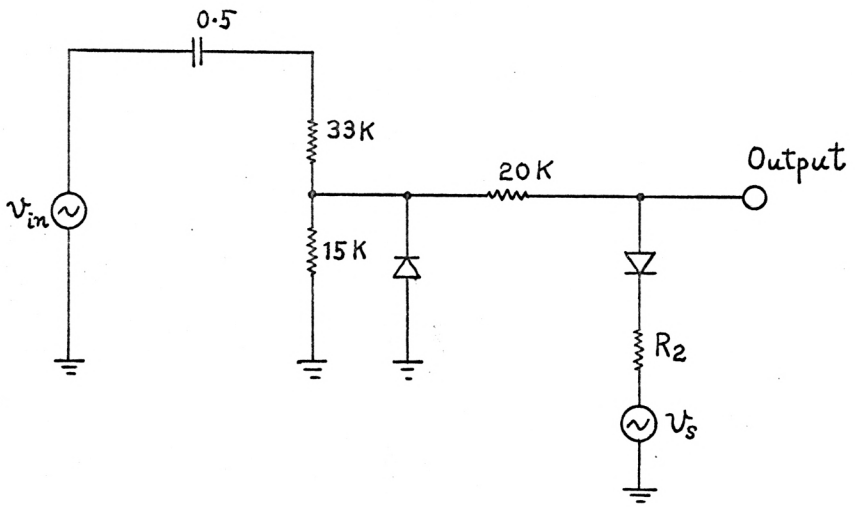

Figure 16. The Modulator Circuit.

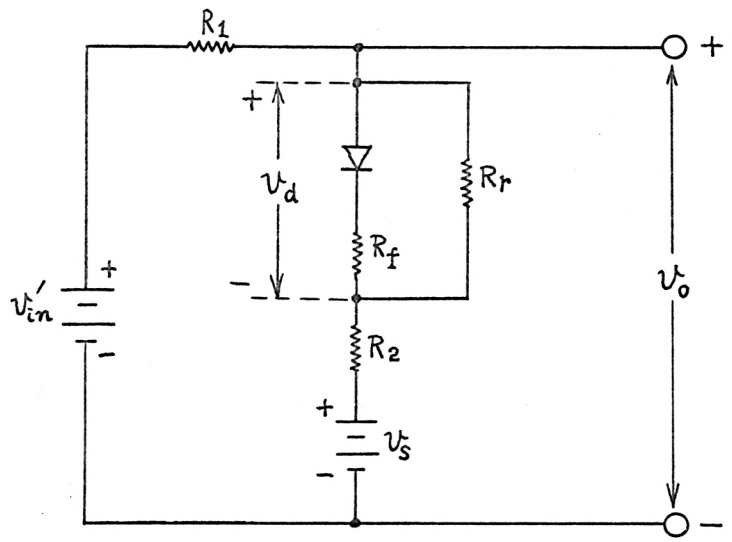

Figure 17. The Equivalent Circuit.

Now, V_o is calculated by substituting the following numerical values in Eq. (93),

$$R_1 = 30\ K\Omega, \quad R_2 = 390\ \Omega,$$

$$R_f = 300\ \Omega, \quad V'_{in} = 15 \text{ volts},$$

$$V_s = 1.5 \text{ volts},$$

as
$$V_o = \frac{30}{30.69} \times 1.5 \left(1 + \frac{0.69}{30} \times \frac{15}{1.5}\right)$$

$$= 1.47\ (1 + 0.23)$$

The error term is appreciable and it causes the modulated signal to have some dc pedestal whose amplitude is inversely proportional to the amplitude of the modulating signal V_s. However, V_s contains some dc component, so that it is possible to reduce the level of the pedestal by clipping off the d c component of the pedestal in the following output amplifier stage. This results in a fairly reasonable amplitude-modulated pulses.

6. The Output Amplifier (V5; 12AT7)

The output amplifier stage of Figure 18 is composed of two cascaded amplifiers. Each unit has an un-bypassed cathode circuit. The negative-feedback effect of the cathode resistor results in a fairly linear input-output characteristic, as shown in Figure 19. The quiescent operating points are chosen as follows.

1st stage $e_k = 2$ volts, $i_p = 2$ m A,

2nd stage $e_k = 4.6$ volts, $i_p = 4.6$ m A.

The gain of each amplifier is six, resulting in the total gain of 36. A clipper circuit is placed between the amplifiers to remove the dc component or the undesired pedestal.

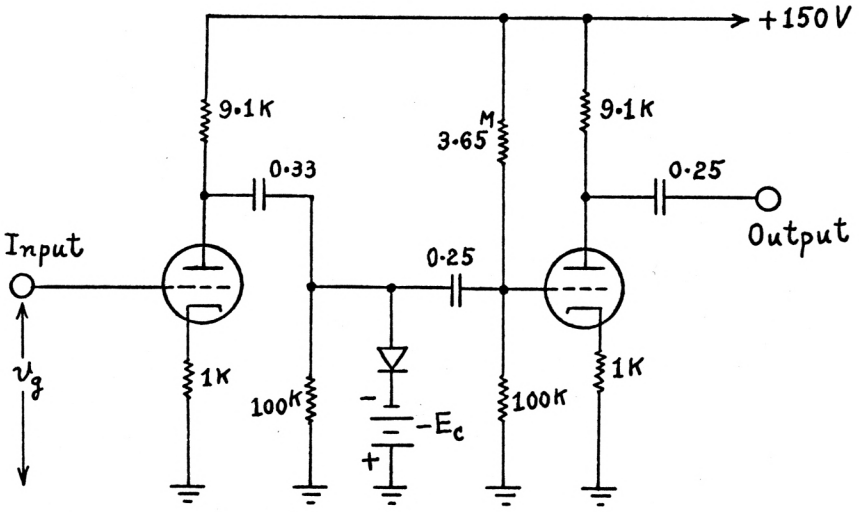

Figure 18. The Output Amplifier Circuit.

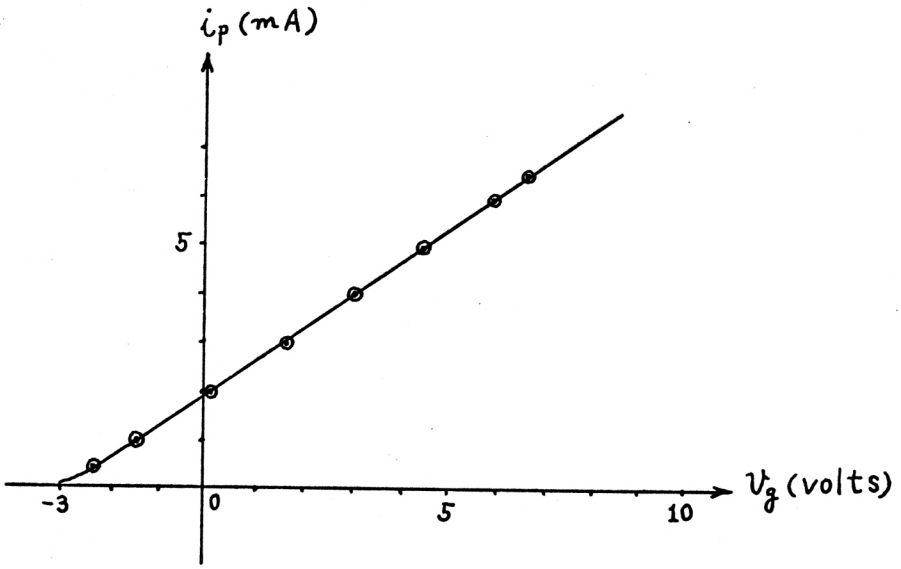

Figure 19. The Input-Output Characteristic of Each Stage.

7. The Gate Circuit

The gate of Figure 20 is used in the output circuit of the output amplifier. A similar gate is also used to process the input pulses to the counter.

The positive going input pulses can go through the input-output branch without any significant loss of amplitude in the absence of a control signal, which is a negative polarity rectangular waveform obtained from the one-shot multi-vibrator V11.

When the amplitude of the gate voltage is larger than that of the input signal, the diode is heavily back-biased and there is essentially no output.

During gating pulse duration, a highly attenuated version of the input appears at the output as shown in Figure 21, but it does not affect the overall performance of the sampler.

8. Schmitt Circuit (V6; 12AT7)

The same Schmitt circuit as V3 is used to amplify and shape (increase the steepness of) input pulses to the counter. This circuit produces trigger pulses with an amplitude of 50 volts for the succeeding counter circuit.

9. The Counter of Scale 6.

The counter of Scale 6 consists of 3 binaries, as shown in Figure 22. Each binary has two stable states (bistable). The binaries under consideration are two-tube devices and the section from which the output is obtained is called the output tube. For convenience the state in which current is flowing in the output tube is called 0. Then the state 1 is the one in which the output tube is cut off.

Prior to the application of the first input pulse, all binaries are in the state 0. The first external pulse when applied to the first binary B_o, causes it to make a transition from state 0 to state 1 as shown in Figure 23.

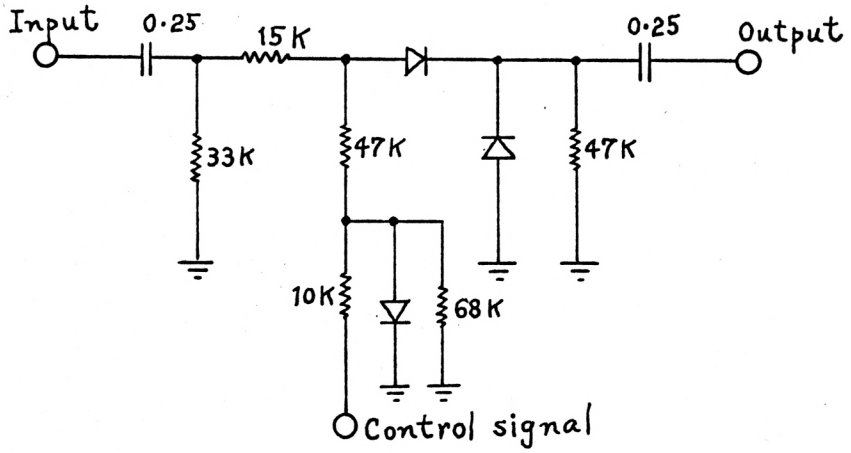

Figure 20. The Gate Circuit.

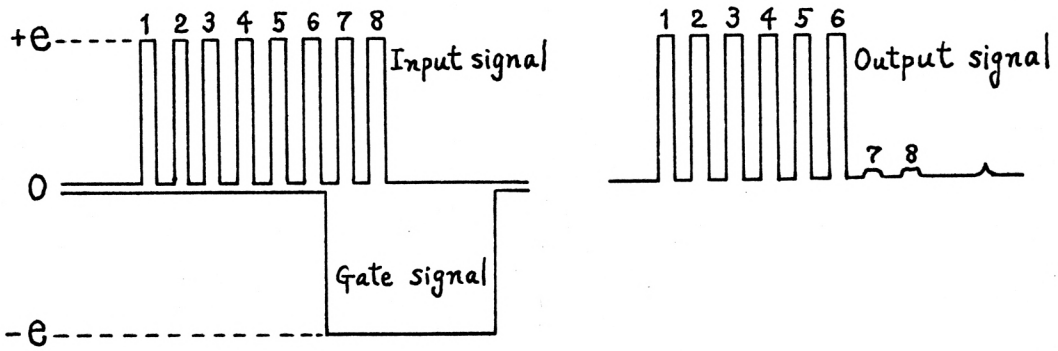

Figure 21. Illustrating Effect of the Gate on the Output.

This transition results in the symmetrical application of a positive step to the second binary B_1 through a capacitor. Since the binary is relatively insensitive to a positive step, the second binary will not respond to the positive step produced by the first binary. The over-all result is that binary B_o has changed to state 1, while the other binaries remain in state 0, as indicated in Figure 23.

The second externally applied pulse causes binary B_o to return from state 1 to state 0. Binary B_1 receives a negative step voltage to which the binary is sensitive and responds by making a transition from state 0 to 1. The binary B_2 does not respond to the transition in binary B_1 because B_2 receives a positive step. A binary does not respond instantaneously to an input step and there is some additional delay before the binary output reaches full amplitude. This feature has been incorporated in Figure 23 by drawing the binary transitions with a finite slope and by starting the transition in a succeeding binary only at the completion of the transition in a preceding binary.

At the fourth pulse, binary B_1 responds and returns from state 1 to 0. Binary B_2 receives a negative step and responds by making a transition from state 0 to 1. This positive step voltage produced by B_2 is differentiated by the coupling network composed of C and R. A negative pulse which results when B_2 goes from state 1 to 0 is ineffective because the coupling triode V10 is held below cutoff by the bias-E_c. The positive pulse is inverted and fed back to P_{1a} of B_1. Since B_1 is in state 0 after the fourth pulse, the negative pulse at P_{1a} will cause transition in B_1. B_1 is forced back to state 1 by this fed-back pulse. Thereafter the counting goes on normally and at the sixth pulse all binaries are again in state 0 and the counting is complete.

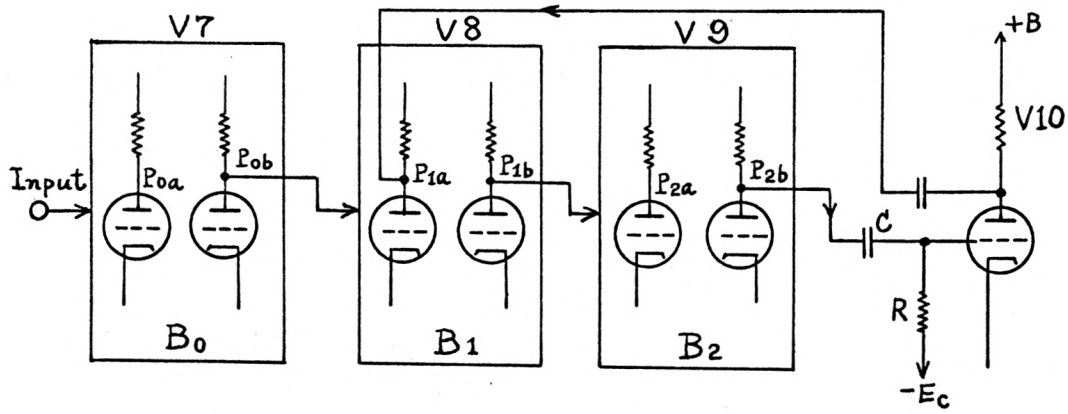

Figure 22. A Scale-of-8 binary chain, modified by Feedback to make a Scale-of-6.

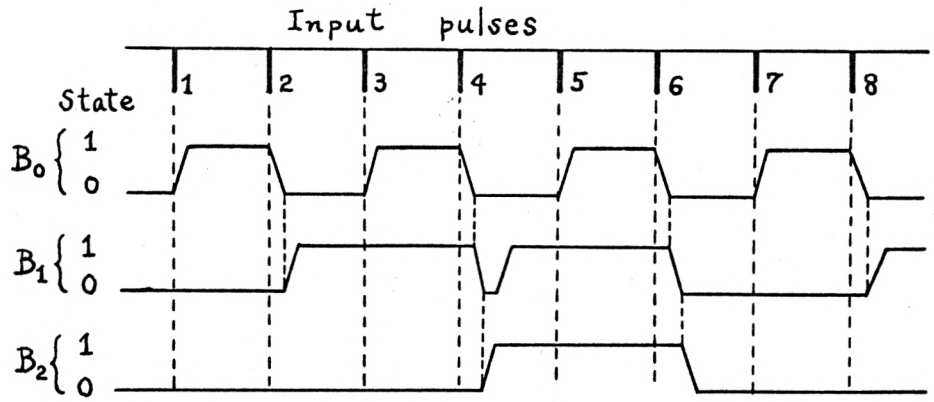

Figure 23. Waveforms Illustration of the Counter.

Now, some detailed analysis of each binary circuit is given.

The First Binary B_o (V7; 5963)

First it is assumed that T_1 is cut off and T_2 is clamped with zero grid-to-cathode voltage. The clamped current is found to be 3.4 m A. The cathode-to-ground voltage is, therefore, $E_k = 12.3 \times 3.4 = 42$ volts. The plate-to-ground voltage of T_2 is

$$E_{p2} = 300 - (27 + 42) \times 3.4 = 65 \text{ volts.}$$

The grid-to-ground voltage of T_1 is

$$E_{g1} = 65 \times \frac{100}{270 + 100} = 17.6 \text{ volts.}$$

The grid-to-cathode voltage of T_1 is

$$E_{gk1} = 17.6 - 42 = -24.4 \text{ volts.}$$

The cutoff voltage is about - 15 volts so that T_1 is well below cutoff, as was assumed at the start. In the absence of grid current, the voltage at the grid of T_2 would be

$$E_{g2} = (300 - 27 \times 3.4) \times \frac{100}{42 + 270 + 100}$$

$$= 208 \times \frac{100}{412} = 50.5 \text{ volts.}$$

Since T_2 clamps when $E_{g2} = 42$ volts, the assumption that T_2 is clamped is seen to be justified. The plate-to-ground voltage of T_1 is

$$E_{p1} = (208 - 42) \times \frac{270}{270 + 42} + 42$$

$$= 185 \text{ volts.}$$

Hence, the plate swing is $E_{p1} - E_{p2} = 120$ volts.

A number of approximations such as that the loading effect of the coupling resistors is negligible, and at clamping the grid-to-cathode voltage is nearly zero have been made. Furthermore, the fact that the cathode resistor carries not only the plate current but also the grid current has been neglected in computing the drop across the cathode resistor. The fact that one uses average tube characteristics, hardly warrant a more exact calculation.

Input triggers are applied to both the grids symmetrically through diodes. The input coupling capacitor (30 p) and the cathode resistor plus 18 K Ω actually constitute a differentiating circuit for the input pulses. The Second Binary B_1 (V8; 5963)

First, assume that T_1 is cut off and T_2 is clamped with a grid-to-cathode voltage equal to zero. Then, the voltages at all nodes can be computed similarly to those for the first binary B_o.

The resulting values are

$$i_2 = 2.6 \text{ m A.}$$

$$E_k = 12.3 \times 2.6 = 32.0 \text{ volts.}$$

$$E_{p2} = 300 - (47 + 47) \times 2.6 = 56 \text{ volts.}$$

$$E_{g1} = 56 \times \frac{100}{270 + 100} = 15.1 \text{ volts.}$$

$$E_{gk1} = 15.1 - 32.0 = -16.9 \text{ volts.}$$

$$E_{g2} = (300 - 47 \times 2.6) \times \frac{100}{47 + 270 + 100}$$

$$= 178 \times \frac{100}{417} = 42.7 \text{ volts.}$$

$$E_{p1} = (178 - 32) \times \frac{270}{47 + 270} + 32 = 156 \text{ volts.}$$

The plate swing = $E_{p1} - E_{p2} = 100$ volts.

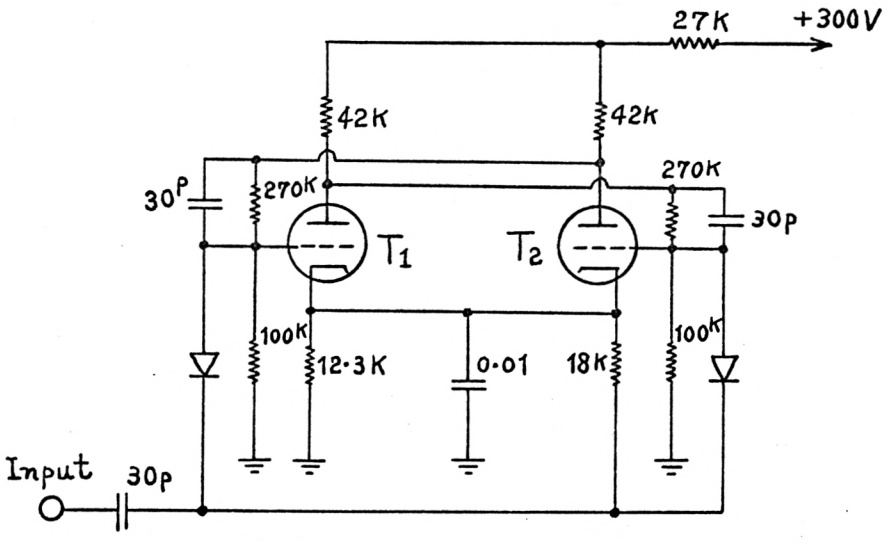

Figure 24. The First Binary B_o.

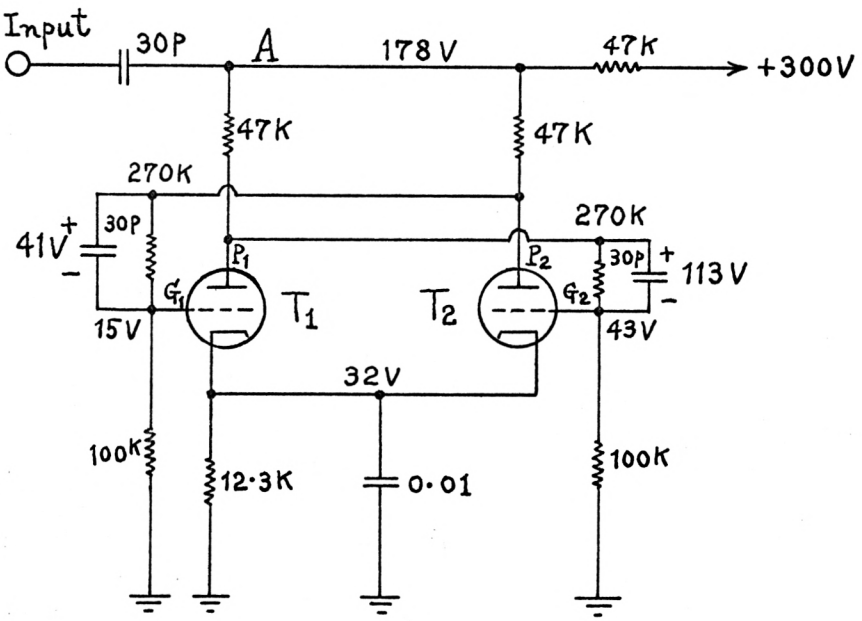

Figure 25. The Second Binary B_1.

The trigger input is applied to the point A in Figure 25.

Now, assume that a negative input step of 100 volts is applied and that the input step has dropped so rapidly that the commutating capacitors have not been able to discharge appreciably. Since the tube T_1 is not conducting, the plate voltage is equal to the voltage at point A, which is 178 - 100 = 78 volts. The voltage at G_2 is equal to the voltage at P_1 minus the drop across the commutating capacitor connected between P_1 and G_2. Hence, G_2 is at -35 volts, and therefore T_2 is cut off. The voltage at P_2 is now also equal to the voltage at point A. As a consequence of T_2 being cut off, the voltage at G_1 rises to a value of 78 - 41 = 37 volts. Since the cathode-to-ground voltage is kept at 32 volts, T_1 is now clamped with zero grid-to-cathode voltage. Hence, a transition has taken place, since T_1 was initially cut off prior to the application of the negative step. After the transition has been completed, the commutating capacitors will interchange voltages.

The Third Binary B_2 (V9; 5963)

The third binary is identically the same as the second binary.

The Feedback Amplifier (V10; 12AT7)

This feedback amplifier shown in Figure 26 is used to differentiate the positive step voltage produced by the third binary and to invert the resulting positive pulse. The amplitude of the negative pulse at the plate can be adjusted by a variable resistor inserted in the bias circuit. The tube is held below cutoff all the time except when the positive pulse is applied.

10. The One-shot Multi-vibrator (V11; 12AT7)

Some calculations show that i_2 is 12.2 m A, and hence $i_2 R_L$ = 6.9 x 12.2 = 84 volts, and $i_2 R_k$ = 3 x 12.2 = 36.6 volts. The maximum allowable voltage

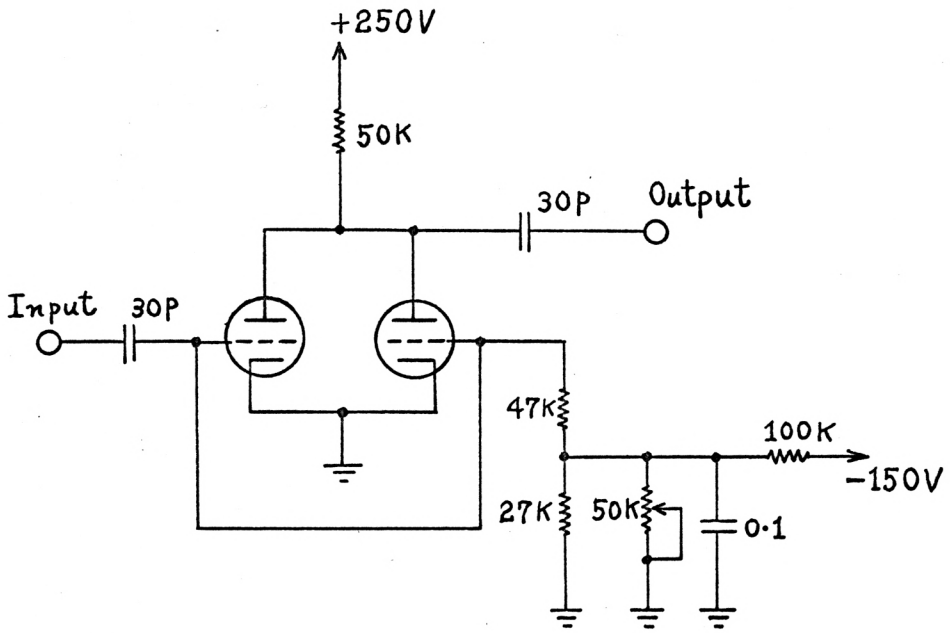

Figure 26. The Feedback Amplifier.

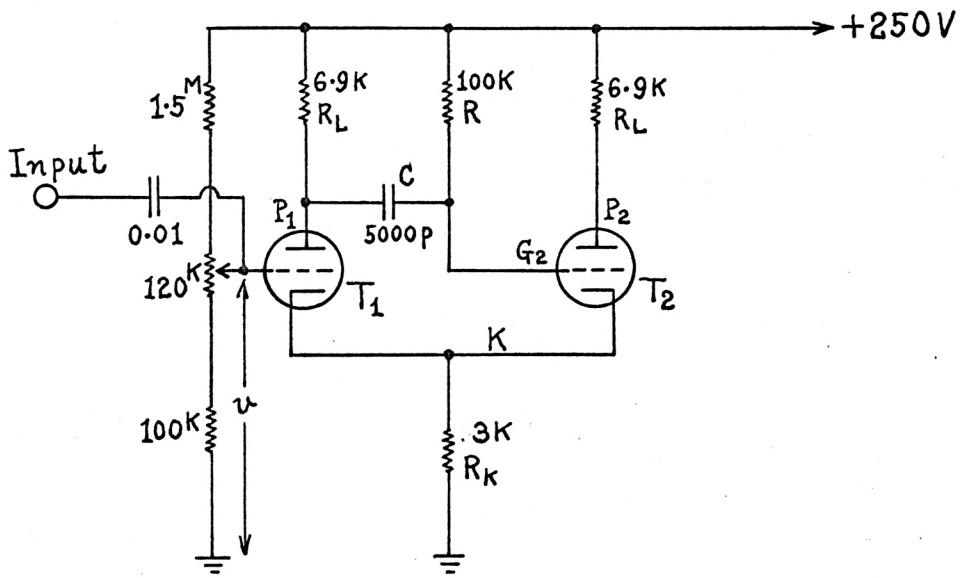

Figure 27. The One-shot Multi-vibrator.

for V, V max, is given by

$$V \text{ max.} = i_2 R_k + E_{col}, \tag{95}$$

Where E_{col} is the cutoff voltage corresponding to a plate-to-cathode voltage of 250 - 36.6 = 213.4 volts. For E_{col} = -5 volts, V max = 36.6 - 5 = 31.6 volts. In order to calculate the minimum voltage V min.,

$$I_o = \frac{i_2 R_k - E_{co2}}{R_L + R_k} \tag{96}$$

must be calculated. Assuming that E_{co2} is approximately equal to - 5.0 volts,

$$I_o = \frac{36.6 - 5}{6.9 + 3} \cong 3.16 \text{ m A.}$$

It appears that E_{co2} is actually the cutoff voltage corresponding to a plate-to-cathode voltage of 250 - 3 x 3.16 = 240.5 volts. Now, from the tube characteristics it is found that a current $I_o = \frac{36.6 - 5.3}{6.9 + 3} = 3.13$ m A flows when the grid-to-cathode voltage is E_{gk1} = -2.9 volts. Hence,

$$V \text{ min} = E_{gk1} + I_o R_k = 6.5 \text{ volts.} \tag{97}$$

$$+ 31.6 \text{ volts} = V \text{ max} > V > V \text{ min} = +6.5 \text{ volts.}$$

Therefore let V be $V = \frac{V \text{ max} + V \text{ min}}{2} \cong 19$ volts.

When T_2 is cut off and V = 19 volts, i_1 is calculated to be 6.85 m A, and

$$i_1 R_L = 47 \text{ volts.} \quad i_1 R_k = 20.5 \text{ volts.}$$

When a positive pulse is applied to G_1 causing V > V max as a result, T_1 is brought into conduction whereas T_2 is cut off. Then, the voltage at G_2 increases exponentially to E_b. All other voltages remain constant until

E_{g2} rises to the cutoff voltage of T_2, Which occurs when $E_{g2} = i_1 R_k + E_{co2}$. At this point the quasi-stable state is terminated, and the voltage settles finally to the quiescent level $i_2 R_k$.

Next, the overshoot voltages are calculated. At the current corresponding to grid clamping (i_2 = 12.2 m A) and plate voltage of 250 - 84 - 36.6 = 129.4 volts, $\mu = 40$, $r_p = 7.7$ K Ω ,

$$r_g = 330\,\Omega \ ,$$

$$\gamma = \frac{(i_1 - I_o)(R_L + R_k)}{R_k + R_L + r_p} \tag{99}$$

$$\cong 0.565.$$

The grid current i_g can be calculated as

$$i_g = \frac{(i_1 - I_o)(R_L + R_k)}{R_L + r_g + (1 + \gamma)R_k} \tag{100}$$

$$\cong 3.0 \text{ m A},$$

and

$$\Delta i_2 = \gamma i_g \tag{101}$$

$$\cong 1.7 \text{ m A}.$$

Hence, at the overshoot the cathode voltage rises to $(i_2 + \Delta i_2 + i_g)R_k$ = 50.7 volts. The calculated waveforms at various electrodes are shown in Figure 28.

Now, the duration of output pulse, T is calculated. The initial value of E_{g2} is $E_i = i_2 R_k - i_1 R_L$ = -11.4 volts. The final value of E_{g2} for $E_f = E_b$ = +250 volts is

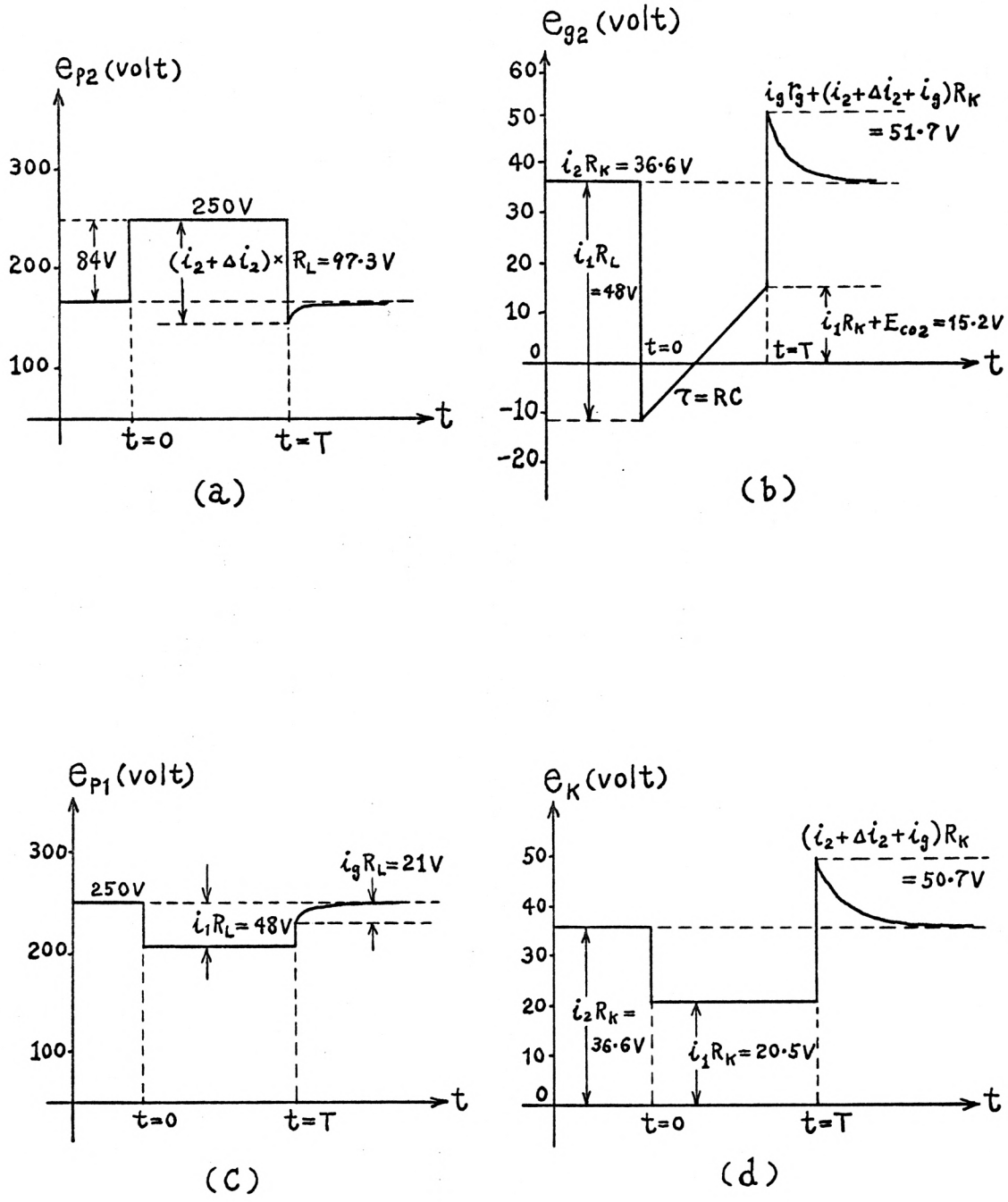

Figure 28. Waveforms of the One-shot Multi-vibrator.

$$E_{g2} = E_f - (E_f - E_i)\, e^{-\frac{t}{cR}}, \tag{102}$$

or
$$E^{-\frac{t}{cR}} = \frac{E_f - E_{g2}}{E_f - E_i}. \tag{103}$$

When $t = T$, $E_{g2} = i_1 R_k + E_{co2} = 15.2$ volts,

$$T = C R \ln \left\{ \frac{E_b - (i_2 R_k - i_1 R_L)}{E_b - (i_1 R_k + E_{co2})} \right\} = C R \times 0.11. \tag{104}$$

Since $C = 5000$ P F and $R = 100$ K Ω ,

$$T = 5 \times 10^{-9} \times 10^{5} \times 0.11 = 55 \times 10^{-6}$$
$$= 55\ \mu \text{ Sec.}$$

Operational Features

An over-all linear gain of approximately 500 was obtained at PRF of 3 kc as shown in Figure 29. The over-all rise time is approximately 4 micro-seconds, and tilt is approximately 3%. The sampled pulses beyond the sixth one appear at the output with highly attenuated amplitude and do not affect the over-all performance of the sampler. The frequency response of the sampler is believed to be essentially flat. The a-c coupling used between the first Schmitt circuit and the succeeding multi-vibrator circuit is not very suitable. The d-c level of the output pulses would have been constant in the case of d-c coupling whereas, in the case of a-c coupling, it is dependent on the pulse width. The dynamic range of the input amplifier, it is believed, can be increased if tubes with higher operating amplitude level are used. In order to simplify the circuit, an unbalanced modulator circuit was used in this system, although it is desirable to use Cowan modulator (balanced type) to eliminate even harmonics of distortion.

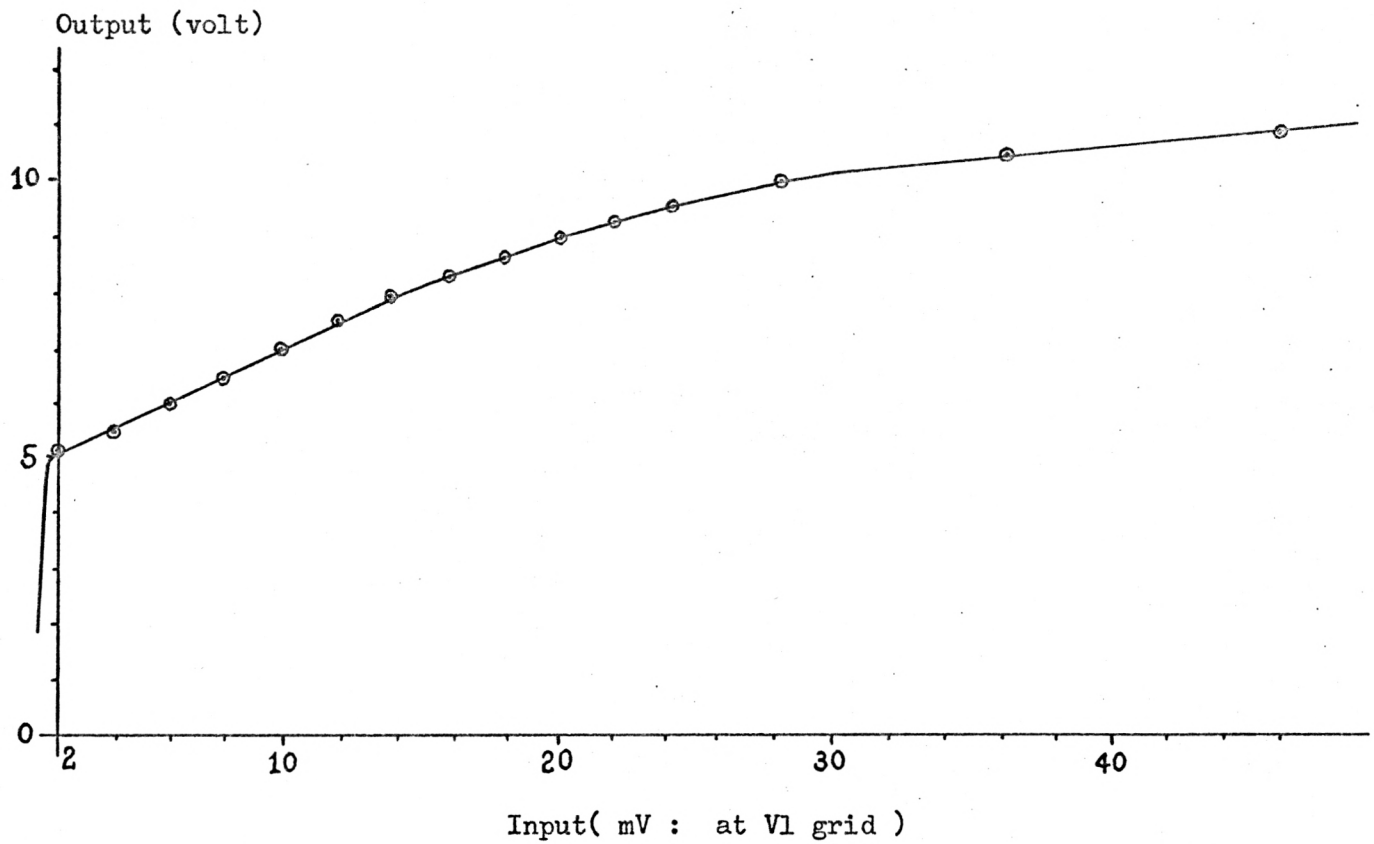

Figure 29. Input-Output Characteristic.

REFERENCES

Andrews, C. L.
Optics of the electromagnetic spectrum. New Jersey: Prentice-Hall, 1960.

Bendat, J. S.
Principles and applications of random noise theory. New York: John Wiley & Sons, 1958.

Cooper, J. A.
Comparison of observed and calculated near vertical radar ground return intensities and fading spectra. M.S. Thesis. Univ. of New Mexico, Albuquerque. Also Engrg. Exper. Station Tech. Rep. EE-10, May 1958.

Davies, H.
The reflection of electromagnetic waves from a rough surface. J. Inst. Elec. Engrs. (London), August 1954. pt. 4, 101, 209-215.

Felsen, L. B., and C. J. Marcinkowski.
Diffraction by a cylinder with a variable surface impedance. Proc. Roy. Soc., A (London), May 22, 1962. 267:329-350.

Fock, V. A.
Generalization of the reflection formulae to the case of reflection of an arbitrary wave from a surface of arbitrary form. Zhur. Eksp. Teor. Fiz. 1956. 20(11):961-978.

Hayre, H. S., and R. K. Moore
Theoretical scattering cross section for near-vertical incidence from contour maps. N. B. S. Res. Journal, September-October, 1961. 65 D(5): 427-432.

Hayre, H. S.
Radar back-scatter theories for near-vertical incidence and their application to an estimate of the lunar surface roughness. D. Sc. Dissertation. Univ. of New Mexico, 1962.

Isakovick, M. A.
Scattering and radiation of waves by statistically inhomogenous and statistically oscillating surfaces. Akust. Zhur., April-June, 1956. 2:146-149.

Lysanov, I. P.
Scattering of sound from plane inhomogenous surfaces with periodically varying acoustic admittance, Acoustic Inst. of the Acad. Sci. USSR, Moscow, 1954. pp. 60-72.

Lysanov, I. P.
An approximate solution of the problem of scattering of sound waves at an irregular surface. Akust. Zhur., 1956. 2:182-187.

Millman, J. and Taub, H.
Pulse and digital circuits. New York: McGraw-Hill, 1956.

Moon, Parry.
Field theory for engineers. New Jersey: D. Van Nostrand Company, 1960.

Moore, R. K., and C. S. Williams, Jr.
Radar return at near vertical incidence. Proc. IRE, Feb. 1957. 45(2): 228-238.

Moore, R. K.
Resolution of vertical incidence radar return into random and specular components. Univ. of New Mexico Engr. Exper. Station Tech. Report EE-6, July 1957.

Pettit, J. M. and McWhorter, M. M.
Electronic amplifier circuits. New York: McGraw-Hill, 1961.

Radio Corporation of America.
RCA receiving tube manual. New Jersey: RCA, 1963.

Rice, S. O.
Mathematical analysis of random noise. Bell System Technical Journal, 1944. 23:81-85.

Schwartz, Mischa.
Information transmission, modulation, and noise. New York: McGraw-Hill, 1959.

Senior, T. B. A.
Impedance boundary conditions for statistically rough surfaces. Appl. Sci. Res., 1960. B8 (5&6):437-462.

Shenk, E. R.
The multivibrator, applied theory and design. Electronics, January 1944. 17:136-141.

Strauss, Leonard.
Wave generation and shaping. New York: McGraw-Hill, 1960.

ELECTROMAGNETIC WAVE SCATTERING AND SOME INSTRUMENTATION OT ITS ACOUSTIC SIMULATION FACILITY

by

TAKUYA KOIZUMI

B. E., Fukui University, 1958

AN ABSTRACT OF
A MASTER'S THESIS

submitted in partial fulfillment of the

requirements for the degree

MASTER OF SCIENCE

Department of Electrical Engineering

KANSAS STATE UNIVERSITY
Manhattan, Kansas

1964

A solution of the scattering of plane electromagnetic waves from an almost plane inhomogeneous terrain with randomly varying impedance, which may be said to represent the amplitude and phase effects of an otherwise rough surface on the reflected wave, is attempted in the first part. An expression of average received power is obtained using Kirchhoff-Huygens' principle and a terrain with Rayleigh distributed impedance, in the sense defined above. It is first assumed to be real and then a general discussion for its complex value is given.

An electromagnetic or an acoustic wave reflected from a rough target surface contains sufficient information about its roughness. This information can be obtained from a return signal if it is sampled for statistical analysis. Use of an electronic sampler results in a great saving of time. Therefore an electronic sampling device for the acoustic simulation facility for radar return of the Department of Electrical Engineering, Kansas State University, is discussed in the second part. This sampler was designed to sample the incoming pulse signal one to six times during the signal duration. Its design and performance are given in detail.